

DOKUZ EYLÜL UNIVERSITY
GRADUATE SCHOOL OF NATURAL AND APPLIED
SCIENCES

GEMMOLOGICAL AND MINERALOGICAL
INVESTIGATIONS AND GENESIS OF THE
KAMMERERITE FROM THE KEŞİŞ
(ERZİNCAN) AND KOP (ERZURUM)
MOUNTAINS

by
Melis Buşra OĞUZER

September, 2012
İZMİR

**GEMMOLOGICAL AND MINERALOGICAL
INVESTIGATIONS AND GENESIS OF THE
KAMMERERITE FROM THE KEŞİŞ
(ERZİNCAN) AND KOP (ERZURUM)
MOUNTAINS**

**A Thesis Submitted to the
Graduate School of Natural and Applied Sciences of Dokuz Eylül University
In Partial Fulfilment of the Requirements for the Degree of Master of Science in
Natural Building Stones and Gem Stones Programme**

**by
Melis Buşra OĞUZER**

September, 2012

İZMİR

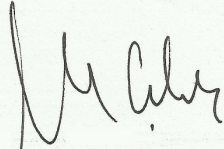
M.Sc. THESIS EXAMINATION RESULT FORM

We have read the thesis entitled **“GEMMOLOGICAL AND MINERALOGICAL INVESTIGATIONS AND GENESIS OF THE KAMMERERITE FROM THE KEŞİŞ (ERZİNCAN) AND KOP (ERZURUM) MOUNTAINS”** completed by **MELİS BUŞRA OĞUZER** under supervision of **ASSOC. PROF. DR. MURAT HATİPOĞLU** and we certify that in our opinion it is fully adequate, in scope and in quality, as a thesis for the degree of Master of Science.



Assoc. Prof. Dr. Murat HATİPOĞLU

Supervisor



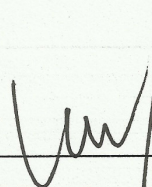
Prof. Dr. Montaz ÇOLAK

(Jury Member)



Prof. Dr. Turgay ONARGAN

(Jury Member)



Prof. Dr. Mustafa SABUNCU

Director

Graduate School of Natural and Applied Sciences

ACKNOWLEDGMENTS

First of all, I would like to express my gratitude and special thanks to my supervisor Assoc. Prof. Dr. Murat Hatipođlu, Dokuz Eylöl University, for his guidance, patience and support, as well as his understanding. I appreciate his time and effort in helping to write this thesis and greatly value his assistance.

The confocal micro-Raman spectrometer device was purchased with the grant of the BAP project, numbered BAP-2009.KB.FEN.051, of Dokuz Eylöl University. Therefore, I wish to give great thanks to Prof. Dr. R. Sami Aksoy, Prof. Dr. İ. Hakkı Bahar, Prof. Dr. Can Karaca, and Prof. Dr. Necdet Türk for their help and support during the purchasing procedure of the spectrometer.

In addition, during the obtaining of the analytical data, I am grateful to Gökhan Gümüő, the director of the Laboratory of Batı Anadolu Cement Factory, for the X-ray diffraction graphics, and also to Asst. Prof.Dr. İbrahim Gündođan and Salim Özcan, from the department of Geological Engineering of Dokuz Eylöl University, for preparing and evaluating the petrographic thin sections.

And, of course, I would like to give my special loves to my parents, for their support and encouragement in everything I do. Thank you!

Melis Buőra OđUZER

**GEMMOLOGICAL AND MINERALOGICAL INVESTIGATIONS AND
GENESIS OF THE KAMMERERITE FROM THE KEŞİŞ (ERZİNCAN) AND
KOP (ERZURUM) MOUNTAINS**

ABSTRACT

Kammererite (chromian clinochlore), in essence, is one of the rarest clinochlore minerals as a sub-variety of large family of the chlorite minerals. Even though it is the monoclinic I1b-2 polytype, with symmetry C2/m, which is one of the most abundant regular-stacking one-layer chlorites occurring in nature, the crystallization of chromian clinochlore is less abundant. Hence, gem-quality magenta colored kammererite which may be formulized as $[Mg_5(Al,Cr,Fe)_2Si_3O_{10}(OH)_8]$ is only found in Turkey worldwide.

Unique loose kammererite crystals were investigated as both mineralogically and gemmologically. Accordingly, some well-known further spectroscopic analytical methods were used to characterize and identify in detail for provenance and genesis of the Turkish kammererite samples.

Firstly, as a structural characterization, in the light of the data obtained from X-ray fluorescence (XRF) and X-ray diffraction (XRD) as well as some essential gemmological measurements and polarizing microscope observations, dispersive confocal (green laser) micro-Raman spectroscopy shows that the strong micro-Raman bands in the kammererite samples with C perpendicular and C parallel axes are peaked at 681, 541, 353, 197, and 112 cm^{-1} . These bands are a result vibrational and librational symmetric and asymmetric stretching and bending modes of molecules, which forms all kammererite structure.

Secondly, as a provenance characterization, photoluminescence and cathodoluminescence spectra show that individual luminescence bands in the kammererite samples are due to mainly chemical defects caused by transition metal

and rare earth elements in the lattice, which are detected by the inductive coupled plasma-atomic emission spectroscopy (ICP-AES).

Finally, these parameters provide positive identification regarding to geographic origin of the original Turkish kammererite, and, give a unique fingerprint for this kind of clinocllore gemstone.

Keywords: Chromian clinocllore, podiform-type chromitite ore deposits, dispersive (green laser) confocal micro-raman spectroscopy, photoluminescence, cathodoluminescence.

**KEŞİŞ (ERZİNCAN) VE KOP (ERZURUM) DAĞLARI KROMİT
YATAKLARINDAKİ KAMMERERİTİN (KROMLU KLİNOKLOR)
GEMOLOJİK VE MİNEROLOJİK İNCELEMELERİ VE OLUŞUM
KÖKENİNİN BELİRLENMESİ**

ÖZ

Kammererit (kromlu klinoklor) esas olarak, geniş klorit mineralleri ailesinin bir alt türü olarak, en nadir klinoklor minerallerinden birisidir. Her ne kadar doğada oluşan en bol düzenli yığılımlı tek tabaka kloritlerden bir olan C₂/m simetrisine sahip bir monoklinik I1b-2 politipi olmasına rağmen, kromlu klinoklorun kristalleşmesi çok nadirdir. Bu yüzden, [Mg₅(Al,Cr,Fe)₂Si₃O₁₀(OH)₈] olarak formülize edilebilen, süstaşı kalitesindeki magenta renkli kammererit, tüm dünya üzerinde sadece Türkiye’de bulunmaktadır.

Özgün tekli kammererit kristalleri, gemolojik ve mineralojik açıdan incelenmişlerdir. Buna göre, iyi bilinen bazı ileri spektroskopik analitiksel metotlar, Türk kammereritinin oluşum yerini ve kökenini detaylı olarak karakterize etmek ve tanımlamak için kullanılmıştır.

Öncelikle, yapısal bir karakterizasyon olarak, X-ışını floresans ve X-ışını kırınımından aynı zamanda bazı önemli gemolojikselle ölçümlerinden ve polarizan mikroskop gözlemlerinden elde edilen veriler ışığında, saçınımsal konfokal (yeşil lazer) mikro-Raman spektroskopisi, C’ye dik and C’ye paralel eksenlerine sahip kammererite örneklerindeki güçlü mikro-Raman bandlarının 681, 541, 353, 197 ve 112 cm⁻¹’lerde piklenmiş olduğunu, göstermektedir. Bu bandlar, tüm kammererit yapısını oluşturan moleküllerinin titreşimselle ve sallantısal simetrik ve asimmetrik gerilme ve bükülme modlarının bir sunucudur.

İkinci olarak, oluşumsal bir karakterizasyon olarak, fotoluminesans ve kathodoluminesans spektraller, kammererit örneklerindeki özgün luminesans bandlarının ICP-AES analizi ile bulunmuş kafesteki geçiş metal ve nadir toprak

elementlerinin sebep olduđu, esas olarak kimyasal hatalarla iliřkili olduđunu göstermektedir.

Sonuç olarak, bu parametreler orijinal Türk kammereritinin cođrafik oluřum kökeniyle ilgili kesin veriler sağlamaktadır, ve bu cins klinoklor süstařı için özgün anahtar iřaretler vermektedir.

Anahtar sözcükler: Kromlu klinoklor, podiform tipi kromit cevher yatakları, saçınımsal (yeřil lazer) konfokal micro-raman spektroskopisi, polarizan mikroskop, fotoluminesans, kathodoluminesans.

CONTENTS

	Page
THESIS EXAMINATION RESULT FORM.....	ii
ACKNOWLEDGEMENTS.....	iii
ABSTRACT.....	iv
OZ.....	vi
CHAPTER ONE – INTRODUCTION.....	1
1.1 Nomenclature and History of Kammererite.....	1
1.2 Advantages of Some Non-Destructive Further Spectroscopic Methods (Micro-Raman and Luminescences) as a Gemstone Characterization.....	3
1.3 Aims and Scope.....	6
CHAPTER TWO – MATERIALS AND METHODS.....	7
2.1 Materials.....	7
2.2 Methods.....	8
CHAPTER THREE – RESULTS AND DISCUSSION.....	15
3.1 Provenance and Geological Setting.....	15
3.2 Polarizing Microscopy (PM).....	17
3.3 X-Ray Diffractometry.....	20
3.4 Geo-Chemistry (XRF and ICP-AES).....	21
3.5 Dispersive (Green Laser) Confocal Micro-Raman (DC μ RS) Spectroscopy...24	
3.6 Luminescence (PL, CL).....	32
3.6.1 Photoluminescence (PL).....	32
3.6.2 Cathodoluminescence (CL).....	35
CHAPTER FOUR – CONCLUSIONS.....	47
REFERENCES.....	39

CHAPTER ONE

INTRODUCTION

1.1 Nomenclature and History of Kammererite

Clinochlore, which is one of the most common members of the chlorite group minerals (Back and Mandarino, 2008), can be divided into three sub-varieties according to body colors and implicational abundance of the main cations (Brown and Bailey, 1963; Bailey, 1988; Grevel et al., 1997; Joswig and Fuess, 1989; Zheng and Bailey, 1989; Theye et al., 2003). These are blackish-green or bluish-green colored clinochlore (ferroan clinochlore) (Rule and Bailey, 1987), yellowish-green or green colored clinochlore (magnesian clinochlore) (Hayes, 1970; Welch et al., 2004), and magenta colored clinochlore (chromian clinochlore) (Lapham, 1958; Brown and Bailey, 1963; Dietrich and Medenbach, 1978; Chadwick, 2008; Farges, 2009). In fact, it is well-known that the name clinochlore was derived from “clino”, which refers to the inclined optical axes and the Greek “chloros,” for “green,” its most typical color (Mitchell, 1979; Schumann, 1984; Arem, 1987; Back and Mandarino, 2008).

Even though rare crystallizations of chromian clinochlore have been reported from the various locations in the world, such as the U.S.A. (California, North Carolina, and Pennsylvania) and Russia (Ural Mountains) (Franklin et al., 1992; Wight, 1996), the most famous and productive source of this mineral exists in a region between Keşiş (Erzincan-Çayırılı) and Kop (Erzurum-Tercan) Mountains in the eastern Anatolia region of Turkey (Figures. 1.1A and 1.1B), as reported in some previously published papers (Brown and Bailey, 1963; M.T.A., 1966; Dietrich and Medenbach, 1978; Chadwick, 2008). These kammererite specimens have already been preserved in museums and private collections around the world, and their origins are acknowledged as the region mentioned above. Therefore, the gem-quality crystals can be specifically called “Turkish kammererite” since they are unique to Anatolia (Figures 1.2 and 1.3).

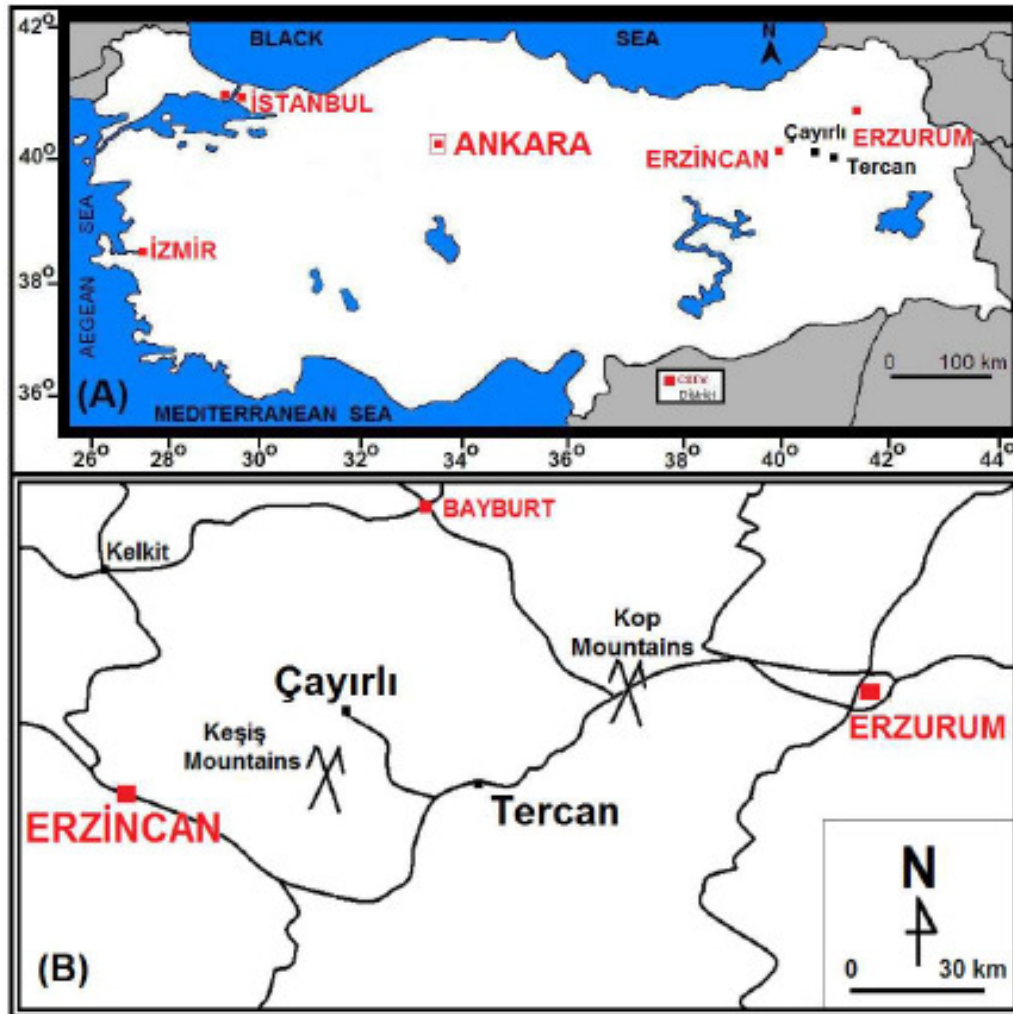


Figure 1.1 Location map showing the most famous region of the podiform-type chromitite ore deposits found between Erzinçan-Çayırılı and Erzurum-Tercan in east Anatolia (A). The deposits are embedded throughout the northeastern ophiolitic belt in the Keşiş and Kop Mountains. The simplified large-scale map of the region including many chromitite deposits with kammererite crystal specimens (B).



Figure 1.2 Kammererite crystals on a chromitite matrix. A chromitite ore fragment on which many kammererite crystals with various dimensions exist (A). Enlarged view of the fragment (B).

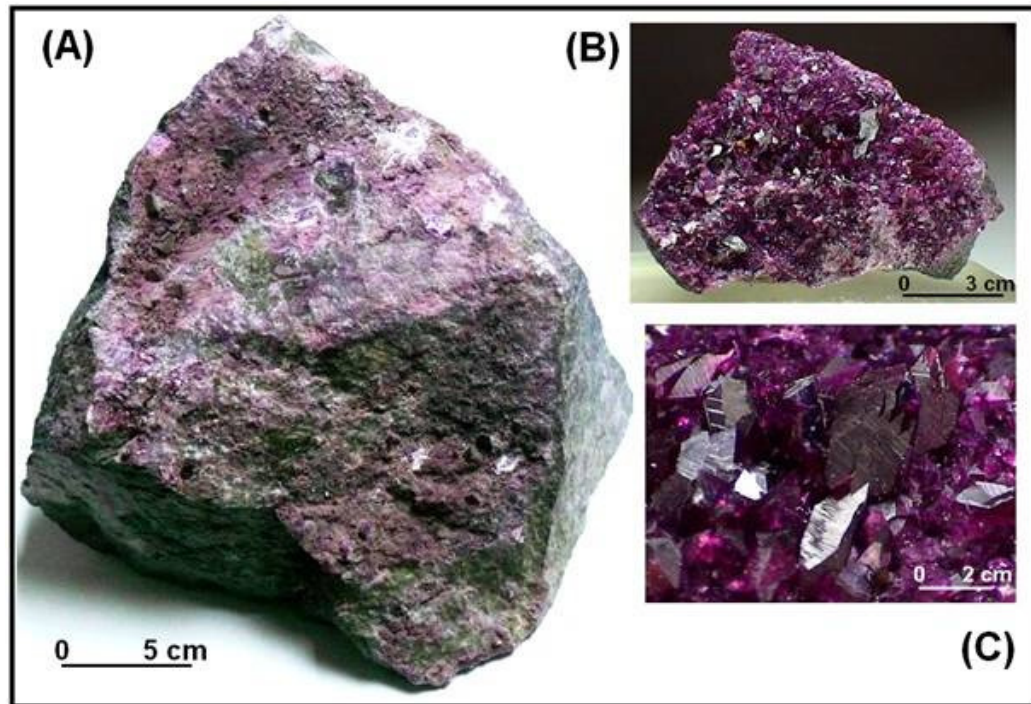


Figure 1.3 Rough ore block composed of chromitite, kammererite, and uvarovite (A), individual kammererite specimens (B) and (C).

1.2 Advantages of some Non-Destructive Further Spectroscopic Methods (Micro-Raman and Luminescences) as a Gemstone Characterization

After the Raman effect was firstly predicted by Smekal in 1923, and later observed experimentally by Raman and Krishnan in 1928 (Raman and Krishnan, 1928), FT-Raman spectroscopy and/or Dispersive(Vis)-Raman spectroscopy have been used as important spectroscopic techniques in condensed matter physics and chemistry to study vibrational, rotational, librational and other low-frequency modes in a system (Deckert et al., 2008; Gucsik, 2009; Vandenabeele, 2010). The frequency wave number of the Raman scattering signal is a reflection of the vibration and rotational modes of the molecule (Wang et al., 1994; Lewis and Edwards, 2001; Šontevska et al., 2007 and 2008; Slodczyk and Colomban, 2010; Vandenabeele, 2010). Raman maps are the images generated from spectra recorded at discrete points of the sample (the recording is automated). They show the variation of any fitted parameter (i.e. intensity, width or position of one band) as a function of the point of analysis. If the mapping is regular and sufficiently tight, one gets a “smart map” of

the parameter (color or contrast scaling) superimposed with the optical image of the probed area. Raman mapping is highly suitable for direct Raman imaging, where a large area of the sample is probed all at once and no fitting is required. More precisely, only photons from a narrow spectral domain are sent to the CCD mosaic and each pixel receives those coming from a given area of the investigated sample. The intensity of the signal thus reveals the presence and location of any substance with a strong Raman signal in the selected spectral window (Gouadec and Colombari, 2007; Colombari and Prinsloo, 2009). The main advantages of Raman spectroscopy are its high information content, lack of sample preparation, and non-destructive nature. In addition, the spectrometer is highly suitable for further gemmological investigations of all kinds of gemstones (Bersani and Lottici, 2010; Fan et al., 2009). Thus, dispersive (green laser) confocal micro-Raman spectroscopy (DC μ RS) is one well-known method for the characterization and identification of gem-minerals (Wang et al., 1994). Additionally, if required, it can be used to distinguish similar colored materials from each other non-destructively. Hänni et al., (1997) have explained some important studies on the gemmological applications of Raman spectrometer. They show how to study by microscope to analyze surface or inner analyses of the material in confocal mode (Hänni et al., 1997). In addition, data base belonging to Raman graphics of gemstones have been published as printed paper by Delé-Dubois et al., (1986), Wang et al. (1994), and as still via internet by RRUFF (2012).

What causes luminescence is a radiation which is emitted when an electron in the structure falls from a high energy level to a lower one. If the crystal dissipates some of the energy as heat, the radiation emitted has a lower energy than the radiation absorbed. Hence, the crystal emits light (Blasse and Grabmaier, 1994; Gaft, 2005; Handerson and Imbusch, 2006). Therefore, it can be summarized that (1) a luminescence encodes the defects that exist in all solid materials, (2) all kinds of minerals show many different types of luminescence relating to the many types of defects (chemical impurities and structural imperfections) they contain, (3) changing the excitation and temperature gives us insights into the causes of mineral and/or material luminescence. Firstly, photoluminescence (PL) is the emission of light from

a mineral and/or material when excited by ultraviolet beams. Photoluminescence spectroscopy is a non-contact and non-destructive method of probing the electronic structure of materials. In essence, when the light is directed onto a sample, a process called photo-excitation can occur, where it is absorbed. The photo-excitation causes the material to jump to a higher electronic state, and will then release energy, (photons) as it relaxes and returns to back to a lower energy level. The emission of light or luminescence through this process is photoluminescence (Blasse and Grabmaier, 1994; Gaft et al., 2005; Gfroerer, 2000; Handerson and Imbusch, 2006). PL (UV-ray induced luminescence) investigations can be used to characterize a variety of material parameters. PL spectroscopy provides electrical (as opposed to mechanical) characterization, and it is a selective and extremely sensitive probe of discrete electronic states. Features of the emission spectrum can be used to identify surface, interface, and impurity levels and to gauge alloy disorder and interface roughness. The intensity of the PL signal provides information on the quality of surfaces and interfaces (Gfroerer, 2000). Secondly, cathodoluminescence (CL) is an optical and electrical phenomenon in which an electron beam is generated by a cathode ray tube, and then impacts on potentially luminescent centres in a material, giving rise to the emission of light. CL (e-ray induced luminescence) provides essential information on provenance, composition, growth fabrics, diagenetic textures, defects in the lattice, and mineral zonation (Marshall, 1988). Peak-width, peak-position, and transition probability of the luminescence centres are influenced by effects such as interactions within the defects themselves, and interaction between defects and the surrounding crystal lattice. The actual CL color is determined by the number and type of emission and quenching centres present. Superposition of several luminescence bands of different intensities can provide quantitative data on the wavelength and intensity of luminescence and the nature of the luminescence centres (Götze, 2000; Townsend and Rowlands, 2000; Habermann, 2002; Gaft et al., 2005; Handerson and Imbusch, 2006).

Finally, these analytical methods approach in a non-destructive and non-invasive way during the investigation of a gemstone sample by simply focusing the scope objective focal point to different depths in the sample (Gucsik, 2009). Therefore,

especially micro-Raman spectroscopy was introduced into the gemmology field in the late twentieth century. Moreover, it is becoming more and more important in mineral research, and many related applications have been reported by many researchers (Hanni et al., 1997; Fan et al., 2009). Thus, it can be stated that dispersive confocal micro-Raman spectroscopy (DC μ RS) as well as luminescence spectroscopy are a well-known method for the analysis of gem-minerals. However, these have not yet been widely used for the identification and determination of kammererite (Gopal, 2004).

1.3 Aims and Scope

This study aims: (1) to give geological formation conditions and establish geographical provenance for the single known deposit of kammererite gem rough; and (2) to publish trustworthy characteristic parameters for these naturally occurring precious Turkish kammererite specimens, including dispersive confocal micro-Raman vibrational bands, X-ray diffraction pattern, gemmological measurements, polarizing microscope images, and major and trace element contents, photoluminescence, cathodoluminescence spectra, and thus (3) to provide Turkish kammererite to be able to distinguish from the other kinds of natural and synthetic kammererites and/or color-enhanced kammererites.

CHAPTER TWO

MATERIALS AND METHODS

2.1 Materials

The investigated kammererite single-crystal samples were obtained from the well-known famous chromitite ore mine (Keşiş Mountains in the Çayırılı-Erzincan region and Kop Mountains in the Tercan-Erzurum region) in the eastern of Turkey (Figure 1.1) which is currently exploited by a mining company. Mainly kammererite and minor uvarovite crystals (Figure 2.1) can be obtained from these chromitites. The dimensions of the crystal samples vary from the size of a pinpoint (about 1 mm in diameter) to a lentil (about 5 mm in diameter). However, it is very difficult to find larger crystals for scientific investigations. These crystals have from transparent to translucent in appearance, generally dark and light magenta coloration, and a perfect cleavage (Figures 1.2 and 1.3).



Figure 2.1 Fine-crystallized specimen including both kammererite and uvarovite Minerals on a chromitite matrix from the well-known famous chromitite ore mine in the eastern of Turkey.

2.2 Methods

In order to verify that Turkish kammererite samples were indeed a Cr-chlorite variety, some basic gemmological (non-destructive) characterization tests by refractometre, hydrostatic balance, and long-wave and short-wave ultraviolet lamps were carried out on the many representative samples (Table 2.1). The tests were performed in the “DGL” Gemmological Testing Laboratory of Dokuz Eylül University.

In addition, from previously published paper by Chadwick (2008), Chelsea filter reaction: Positive (pink), *Inclusions under polarizing microscope*: Numerous fractures and cleavages, as well as crystals, needles, and clouds of tiny pinpoint inclusions. *Absorptions by UV-Vis-NIR spectroscopy*: transmission windows in the blue and red portions of the spectrum, which are consistent with the purplish red color of the samples.

Table 2.1 Some essential gemmological measurements of Turkish kammererite.

Basic gemmological measurements	Turkish Kammererite Monoclinic <i>I1b</i> -2 polytype, with symmetry <i>C2/m</i>
Specific Gravity (SG)	S.G.= 2.69
Optical Character Refractive Index (RI) Double Refraction	Anisotropic, Biaxial (+) $N\alpha=1.572$ $N\beta=1.581$ $N\gamma=1.592$ D.R.= 0.009
Luminescence against UV excitation	Inert
Pleochroism	Fuchsia and magenta tones, lilac
Cleavage	{001} perfect
Fracture	Uneven-Flat surfaces (not cleavage) fractured in an uneven pattern
Diaphaneity	Transparent to translucent
Hardness	2-2.5
Lustre	Vitreous-Pearly, Streak: white

The specific gravity (SG) values of the many representative kammererite samples were measured in this study using an electronic balance scale (measurement

sensitivity of 0.001) with an SG kit, based on the formula ($SG = W_{\text{air}} / W_{\text{air}} - W_{\text{water}}$) (Figure 2.2). The optical character, optical sign, and refractive index values of the representative kammererite samples were determined using an Eickhorst SR/XS standard refractometre device with an optical contact liquid of 1.79 RI, and a quartz lamp with a wavelength of 589 nm (Figure 2.3). Ultraviolet (UV) luminescence reactions of the representative kammererite samples were observed using a System Eickhorst UV 240 shortwave (255 nm) and long wave (366 nm) 4W UV lamp (Figure 2.4). Consequently, all these results indicate that the investigated mineral species is a typical clinochlore variety belonging to the chlorite mineral's group.

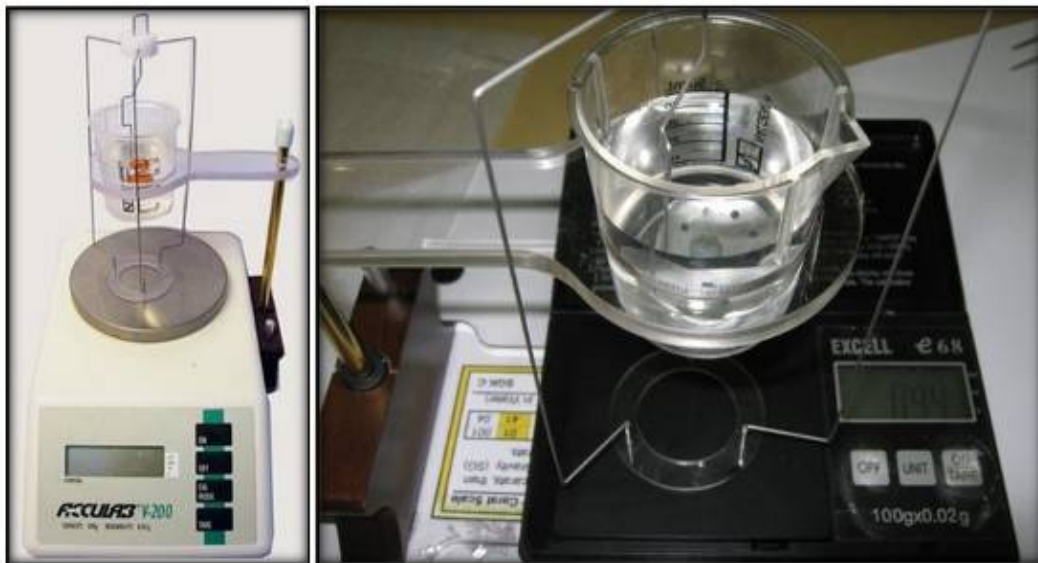


Figure 2.2 Gemmological specific gravity apparatus for sensitive measurement of the weight in air and the weight in water of Turkish kammererite.

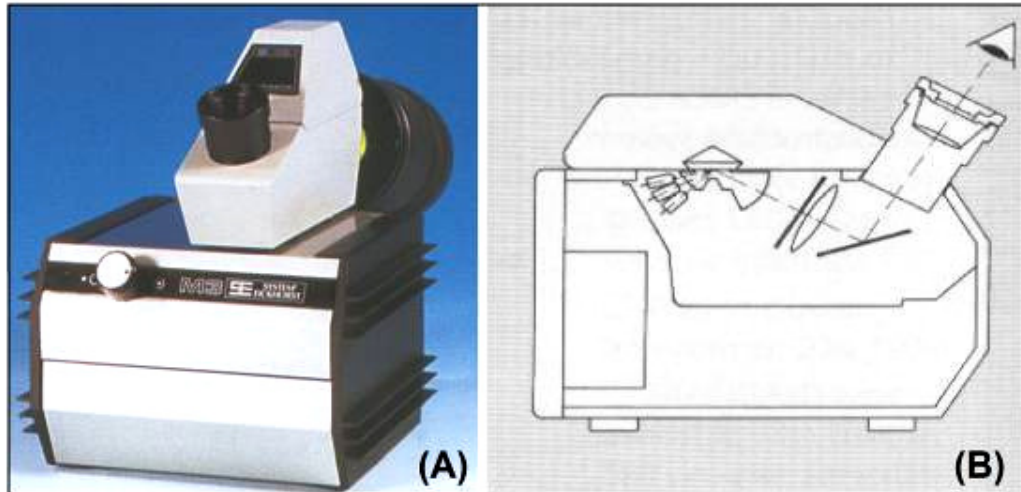


Figure 2.3 Perspective (A) and longitudinal section (B) images of the gemmological standard refractometre device used for measuring the refractive index values of Turkish kammererite, including optical character and optical sign with an optical contact liquid of 1.79 RI, and a quartz lamp with a wavelength of 589 nm.



Figure 2.4 Gemmological ultraviolet lamps for measuring the long and short luminescence reactions of Turkish kammererite.

Polarizing microscope images of thin sections of Turkish kammererite were obtained using an Olympus BX41 binocular polarizing microscope with a high intensity 6V, 30W halogen light source combined with U-CPA and U-OPA optical systems, after thin sections of the samples had been mounted on glass lamellae

(Figure 2.5). For the digital images, the microscopic magnifications (MM) are as follows; X4 (a combined magnification of X0.4 objective and X10 ocular) and X2 (a combined magnification of X0.2 objective and X10 ocular) under the crossed nicols (+N) (active polarizer and analyzer) and parallel nicols (||N). The polarizing microscope investigations were performed in the Optical Mineralogy Laboratory of the Department of Geology at Dokuz Eylül University.

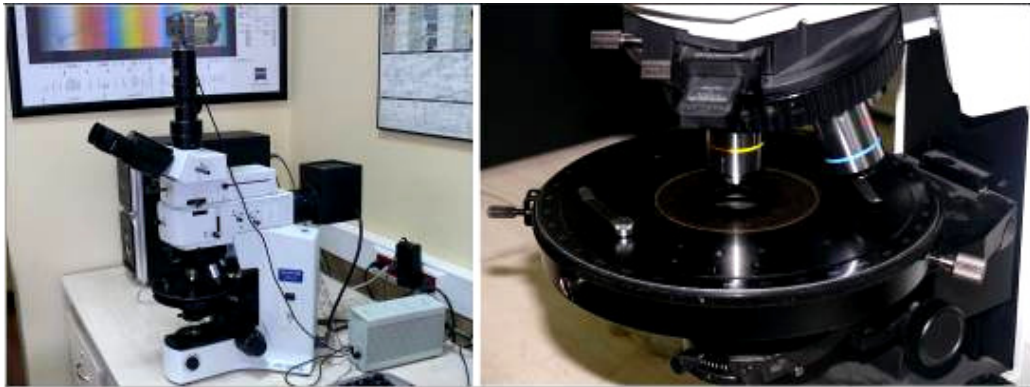


Figure 2.5 Olympus BX41 binocular polarizing microscope with a high intensity 6V, 30W halogen light source combined with U-CPA and U-OPA optical systems, used in this investigation.

The structural pattern of Turkish kammererite was detected from X-ray powder diffraction patterns made using a Cubi-XRD device with a Cu tube and a graphic monochromator. The representative samples were analyzed with Cu radiation and a 0.3 mm collimator at atmospheric pressure for 10 minutes each. The instrument used 1.54056 Å for K-Alpha1 and 1.54439 Å for K-Alpha2, operating in ambient temperature at 40 kV and 30 mA. The initial and final wavelengths for the samples were performed at the scanning rate of 0.33°/min for 2θ from 5° to 70°, and a tolerance range of ± 0.01 . The d-spacing [Å] diffraction matchings using the comparative matching technique are based on the positions of peaks with relative intensities [$\%(I/I_0) \geq 2$], 2-theta values below 70°. X-ray diffraction patterns were recorded in the Material Research Laboratory of the Batı Anadolu Cement Factory in İzmir.

Chemical analysis of Turkish kammererite was made by X-ray fluorescence (XRF) for major oxides, inductively coupled plasma-atomic emission spectroscopy (ICP-AES) for trace elements, and WST-SIM for determination of ignition losses. These analysis was certified with the code number ‘‘IZ10044112’’, under contract by the accredited ALS Chemex Laboratory in Canada.

The dispersive confocal micro-Raman spectroscopy of Turkish kammererite was performed on a dark background at room temperature using a HORIBA Jobin Yvon Scientific X-PLORA dispersive confocal micro-Raman spectrometer (DCuRS) with a high throughput integrated spectrograph (Figure 2.5). The spectrometer uses one laser excitation of about 532 nm (green light). Spectral manipulation as baseline adjustment was carried out using the software of the device. The Raman record was obtained in the ‘‘DGL’’ Gemmological Testing Laboratory of Dokuz Eylül University in İzmir.

Photoluminescence (PL-3D) morphology of Turkish kammererite was obtained by using a Fluorolog 2T Fluorescence Spectrometer. A Xe-lamp with a wavelength range of approximately 370 to 850 nm and a temperature range of approximately 230 to 330 K was used as excitation. Luminescence can be either after excitation (where the primary beam has higher energy than the secondary light) or after stimulation (where the primary beam has less energy than the luminescence). These wavelengths were selected using a monochromator (Spex 1681 0.22 mm) and emission analysed with a Spex 1680 Double Spectrometer. The detector is a front-illuminated open-electrode CCD (200-1100 nm). Finally, the photoluminescence (PL-3D) images of the samples were originally taken by Axum 5.0 software. Later, the PL-3D morphology was converted into a PL-2D counter map using Surfer 8.0 software. Next, many PL-2D graphics were produced from the PL-3D morphology using Surfer 8.0 and Grapher 8.4 software.

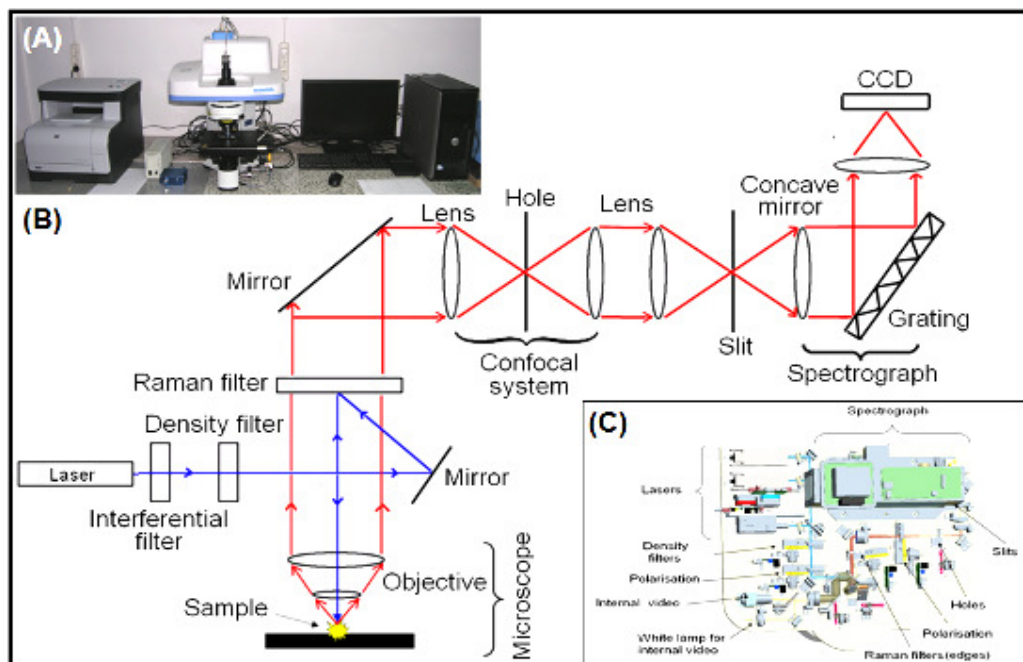


Figure 2.6 The dispersive confocal micro-Raman spectrometer used in this study (A), its schematic diagram (B) and description (C).

Cathodoluminescence time resolved spectroscopy was performed on Turkish kammererite. The current was 20 mA. The acceleration potential was the energies of 14 and 24 keV electrons corresponding to an incident power density of $0.8 \mu\text{Acm}^{-2}$ at room temperature. The primary electron beam is normally pulsed using a Thandor TG501 5 MHz function generator as a function with the frequencies of 90, 180, 360, and 900 Hz at 14 keV, and with the frequencies of 90, 180, 360, 900, and 9000 Hz at 24 keV, except for the lifetime measurement. The CL response was gated using an EgandG Ortholoc-SC 9505 2-phase lock-in amplifier, and a cooled red-sensitive photomultiplier tube. It is worth noting that the broad diameter of the beam significantly reduces any instability due to secondary electron emission. The light coming from the samples was focused via a quartz lens onto the entrance slit of a grating monochromator with $f/4$ light collection, and detected with a blue-sensitive photomultiplier tube (PMT, EMI 9813Q). The quantum efficiency of EMI 9813Q is between 15% and 25% in the range of 250 nm to 800 nm. Two different measurements can be performed on the samples, using the alternating current (AC) and the direct current (DC) generated in the system. DC measurements can potentially record optical signals from the electron gun source, but this is rejected in

the AC operating mode. However, only Alternating Current (AC) measurements were used on the samples at room temperature during the experiment. In AC measurement, an Ortholoc-SC9505 two-phase lock-in amplifier was employed. This instrument was used in normal mode where it performs in exactly the same way as an ordinary lock-in amplifier, i.e. only one channel is needed. The spectral lines obtained using a mercury (Hg) discharge lamp and Nd:YAG laser were used in wavelength calibration using 3 mm entrance and exit slits on the monochromator. The wavelengths of the spectral lines used in the calibration are 405, 436, 546 and 577 nm for the Hg and 633 nm for the He-Ne laser. The efficiency of the spectral response of the whole system was obtained by recording the spectrum of a tungsten lamp used with the same aperture as in the wavelength calibration. Hence, it was possible to correct the wavelength dependent sensitivity of the system. The electron beams were chopped at frequencies from 9 to 900 Hz, and the photomultiplier output was measured on a lock-in amplifier. The wavelength resolution was set at 5 nm for the CL measurements. Due to the changes in ion beam energy, the current density may modify the emission spectra and intensity.

CHAPTER THREE

RESULTS AND DISCUSSION

3.1 Provenance and Geological Setting

In this study, the geology of the region surrounding the chromitite ore deposit in the Keşiş and Kop Mountains, in which Turkish kammererite specimens exist, was re-investigated, taking into account previous field observations.

Even though there are many chromitite deposits in Turkey (M.T.A., 1966), the most productive kammererite-bearing sources in Turkey are present in the eastern Anatolia region where the podiform-type chromitite ore deposits (Demirmen, 1965; Uysal et al., 2007) run in a line through the Keşiş Mountains (near Erzincan-Çayırılı) and Kop Mountains (near Erzurum-Tercan) (Dietrich and Medenbach, 1978; Wight, 1996) of the northeastern ophiolitic belt (Petrascheck, 1958; Temiz et al., 2002; Rızaoğlu et al., 2006) (Figures 1A and 1B).

Geological field investigations indicate that these kammererite crystals occurred due to remobilization as a result of four metamorphic processes (extraction, mobilization, migration, and re-crystallization) in an aqueous complex. The Cr, Mg, Fe, Al, and Si ions were migrated step-by-step via the redistribution of chemical bonds. They are, in fact, a secondary hydrothermal alteration product of chromitites and also amphibole, pyroxene and biotite minerals (Uysal et al., 2007) in the surrounding peridotitic (partially serpentinitic) rocks (Demirmen, 1965). The chromitite matrix has a podiform ore occurrence (Petrascheck, 1958; Kadayıfçı and Kolaylı, 2009) which is embedded throughout the northeastern ophiolitic belt (Demirmen, 1965). Similarly, remobilization occurrences in the podiform chromitites from southeastern Australia were reported by Franklin et al. (1992).

On the large scale, the northeastern Anatolia section of Turkey is characterized by two large tectonic units, namely the Eastern Pontides and the Eastern Taurides (Şengör ve Yılmaz, 1981; Okay and Şahintürk, 1997). These two tectonic units are

separated by the Ankara-Erzincan suture zone (Özener et al., 2010). The Eastern Pontides, interpreted as a part of the Sakarya Zone (Okay and Şahintürk, 1997), are known as an active continental margin of Laurasia, which was formed as a result of northward subduction of Neotethys during the Late Cretaceous (Şengör ve Yılmaz, 1981; Okay and Şahintürk, 1997; Rice et al., 2006). Whereas the Taurides to the south are represented by the Tauride Carbonate Platform, the Pontides are envisaged as one or several micro continents that rifted from Gondwana during Early Mesozoic time (Şengör ve Yılmaz, 1981). They display intact successions ranging from Late Precambrian to Early Cenozoic. The Ankara-Erzincan suture zone includes large bodies of ophiolites and ophiolitic melanges in northeastern Anatolia.

The kammererite-bearing region between the Keşiş Mountains to the southwest and the Kop Mountains to the northeast has a complex geological setting.

In this basin, a wide ophiolitic complex was situated tectonically on the Early Cretaceous aged limestones (Temiz et al., 2002; Rızaoğlu et al., 2006; Rice et al., 2006). There are many chromitites in these peridotites of the ophiolitic complex, some of which were serpentinized. The chromitites of the quarries on the slopes of the Keşiş and Kop Mountains are found as masses with tectonic surfaces or nodules, which were cracked, rounded and returned to a sausage-like (boudinage) structure. The average tenor of Cr₂O₃ is 50%. Mainly kammererite, but also uvarovite minerals are found in these chromitites (Petrascheck, 1958; M.T.A., 1965; Demirmen, 1965; Uysal et al., 2007; Kadayıfçı ve Kolaylı, 2009).

It is well-known that chromium-rich rare mineral occurrences are in result of the hydrothermal alteration and remobilizing process (Franklin et al., 1992; Caillaud et al., 2009) of ophiolitic (ultrabasic) rock varieties. Anatolian kammererite crystals also have such a genesis in this region of Turkey. Demirmen (1965) stated that smectite (a rare variety of the clay minerals) existed in the Erzincan-Çayırılı basin (Demirmen, 1965). This mineral formation provides important evidence for the alteration of ultrabasic rocks, and as a result, for some remobilized rare mineral occurrences in the region (Uysal et al., 2007). In another related study on trace metal

distribution from a serpentinite weathering, Caillaud and his colleagues stated that the distributions of four trace metals (Ni, Cr, Mn and Co); derived from a natural trace metal-bearing rock (serpentinite), are relatively enriched in weathered horizons compared to inside the rock, in the same way, as iron, aluminium, and magnesium are largely leaching. Silicates (serpentine and clinocllore) contain Cr, Ni and Mn whereas oxides concentrate Co and Cr. In the first weathering stages, Ni and Cr are concentrated in secondary clays, especially in Fe-montmorillonite (derived from some serpentine minerals) and in trioctahedral vermiculite (derived from chlorites) respectively, whereas Mn and Co are mainly used to constitute secondary oxides (Caillaud et al., 2009). Franklin and his colleagues investigated the remobilized occurrences of chromian clinocllore in the Coolac Serpentinite Belt, which is a sub vertical, alpine-type ultramafic body within the Palaeozoic Lachlan Fold Belt of eastern Australia, and additionally, they revealed that chromium was mobilized over a substantial temperature interval for the chrome-bearing phases including ferrochrome, uvarovite (formation temperature 500°C+) and chromian clinocllore (formation temperature ~300°C) (Franklin et al., 1992).

3.2 Polarizing Microscopy (PM)

Thin sections at magnifications of X2 and X4 under a polarizing microscope show the crystalline coarse-grained material of Turkish kammererite (Figures 3.1 and 3.2). Crystalline habit is clearly seen as the monoclinic *I1b-2* polytype, with symmetry *C2/m*, which is one of the most abundant regular-stacking one-layer chlorites occurring in nature (Dietrich and Medenbach, 1978; Bailey, 1988; Joswig and Fuess, 1989; Zheng and Bailey, 1989; Welch and Marshall, 2001; Zanazzi et al., 2007; Chadwick, 2008).

The detailed observation of the texture in the examined images reveals a variety of stacking sequences, distortions from geometrically ideal structures, and order-disorder relationships (Zheng and Bailey, 1989; Zanazzi and Pavese, 2002; Zanazzi et al., 2006 and 2007).

It is well-known that chlorite polytypism represents four different chlorite layer types. It is reported that at least three of these are present in natural chlorite specimens (Brown and Bailey, 1963; Joswig and Fuess, 1989; Walker, 1989; Weiss, et al., 1992).

Even if a few natural chlorites have regular 1-layer, 2-layer, or 3-layer sequences, most chlorites crystallize with a semi-random sequence involving one particular layer type that is especially stable because of minimum cation repulsion and short inter-layer OH-O bond lengths (Brown and Bailey, 1963; Brown, 1976; Zheng and Bailey, 1989; Zanazzie et al., 2007; Walker, 1989).

It is stated that the structure of Turkish kammererite has a regular sequence of one of the most common layer types, designed *I**b**-2* polytype in the chlorite terminology (Dietrich and Medenbach, 1978; Bailey, 1988; Chadwick, 2008).

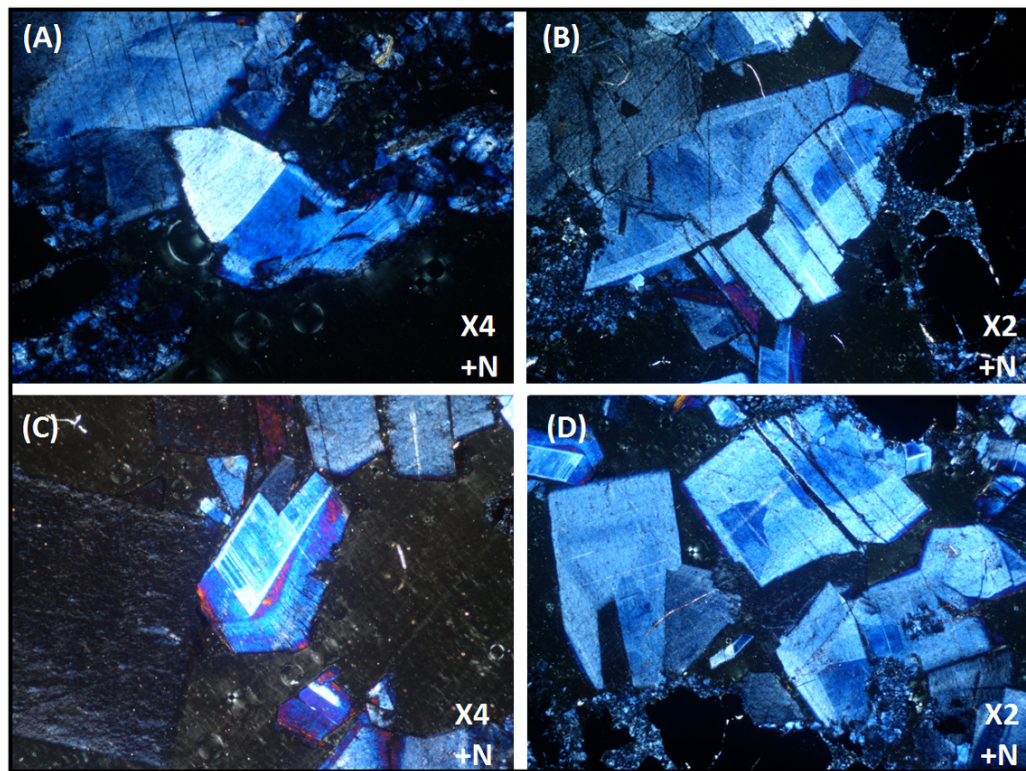


Figure 3.1 Microphotographs of Turkish kammererite, viewed in crossed-polarized light at magnifications of X4 (**A** and **C**) and X2 (**B** and **D**). The width of the images is 0.65 mm.

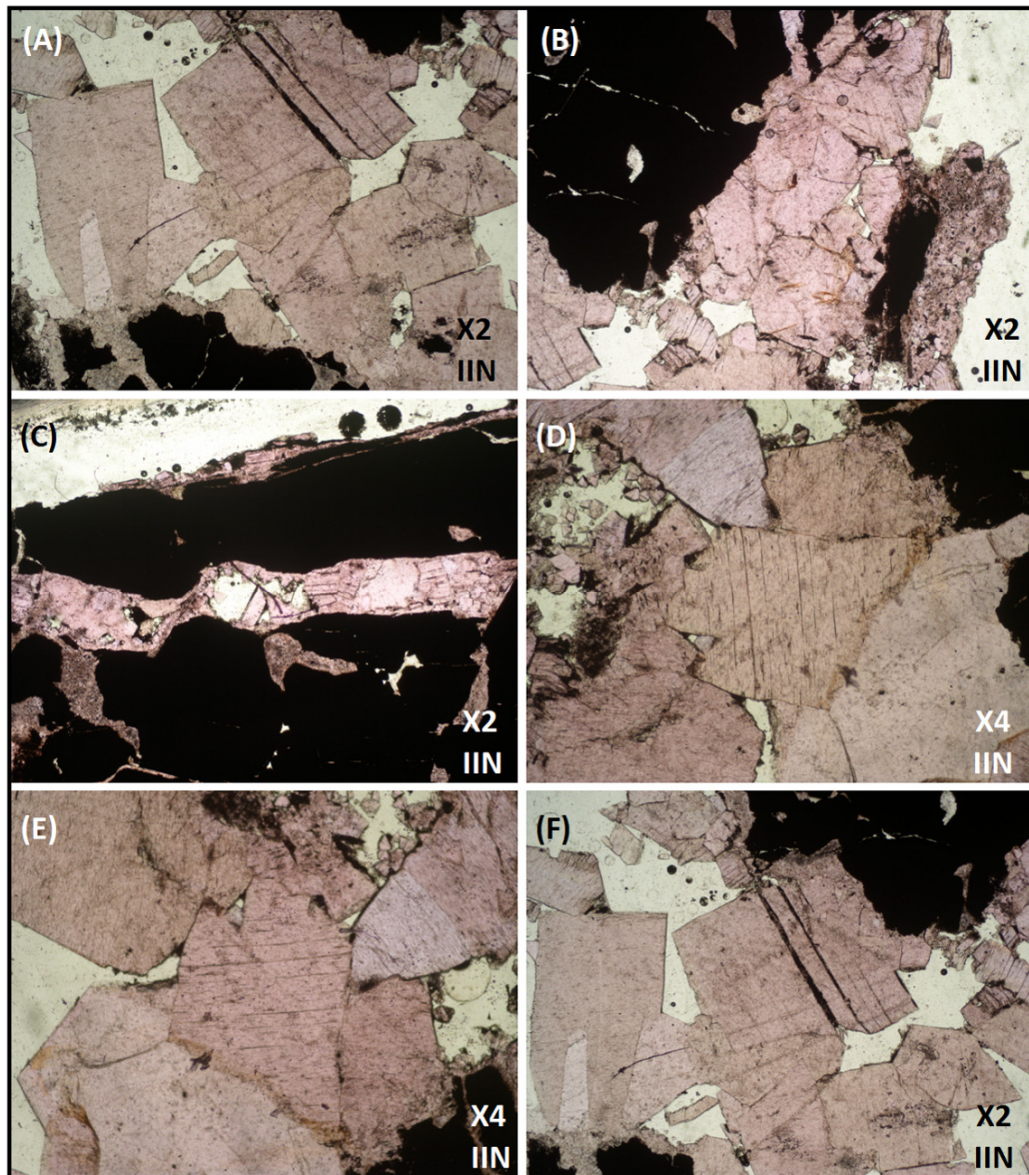


Figure 3.2 Microphotographs of Turkish kammererite, viewed in parallel polarized light at magnifications of X4 (D and E) and X2 (A, B, C and F). The width of the images is 0.65 mm.

3.3 X-Ray Diffraction (XRD)

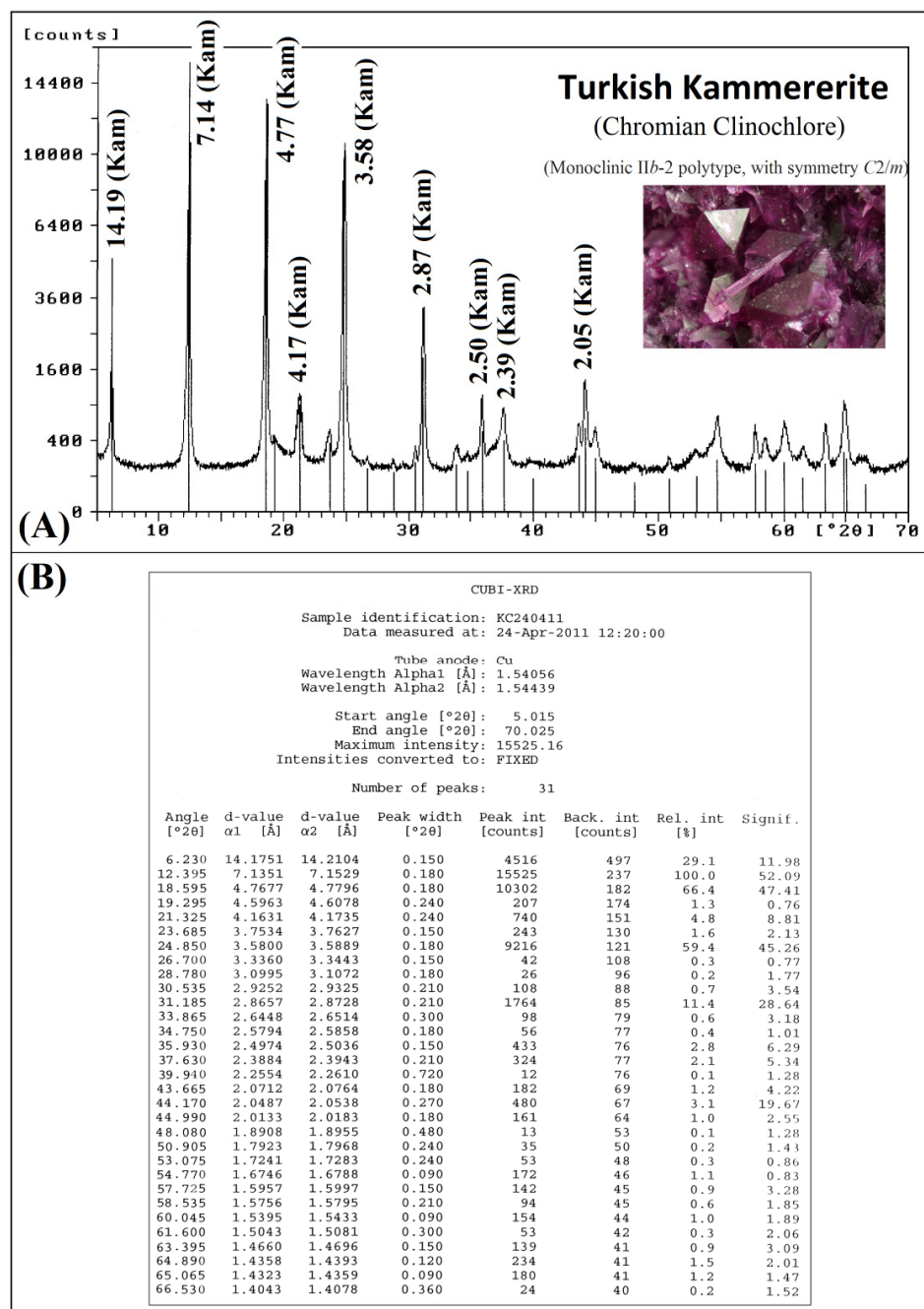


Figure 3.3 The XRD pattern of the representative Turkish kammererite (A), according to the numerical experimental XRD data (B), showing the labels of the single or overlapped peaks of the base clinocllore building phase components. The positions of peaks with d-spacings [Å] and relative intensities [%(I/I_0)] are labelled for $\geq 2\%$ of 2-theta values below 70 degrees.

Numerical data obtained from XRD analysis of the representative Turkish kammererite sample was tried to be matched to that of ideal clinochlore mineral compiled from the some important crystal structure databases (AMCSD, 2012; RRUFF, 2012; WEBMINERAL, 2012) as well as some previously published related papers (Lapham, 1958; Dietrich and Madenbach, 1978; Rule and Bailey, 1987; Wight, 1996; Theye et al., 2003; Gopal, 2004; Welch et al., 2004), using a comparative matching technique for XRD data. Hence, the investigated structure was confirmed as clinochlore (Figure 3.3).

The matched clinochlore building phases were labelled with specific abbreviation to help the readers as (Kam) for kammererite on the given X-ray diffraction pattern (Figure 3.3). As it can be seen in the representative XRD pattern, nine essential X-ray peaks are characteristic.

3.4 Geo-Chemistry (XRF and ICP-AES)

Chemical analysis of the representative kammererite sample was carried out both X-ray fluorescence (XRF) for major oxides and inductively coupled plasma-atomic force microscopy (ICP-AES) for trace elements, and their comparative results have been given in Table 3.1. As seen, chemical bulk analyse verify that Turkish kammererite occurs in the ultrabasic-characterized peridotitic (partially serpentinized) host rock according to especially SiO₂ (6.55%), Al₂O₃ (12.43%), CaO (0.05%), MgO (18.07%), Na₂O (0.05), and K₂O (0.03%) concentrations.

It is well-known chromium-rich rare mineral occurrences in the result of the alteration and remobilizing process (Franklin et al., 1992) of ophiolitic (ultrabasic) rocks, and the similar ones (Komov et al., 1994). Kammererite has such a genesis in the Keşiş and Kop Mountains region in Turkey. Demirmen (1965) stated that there was smectite (a rare variety of clay minerals) in the Erzincan-Çayırılı basin. This mineral formation is an important evidence for the alteration of ultrabasic rocks, and as a result, for some remobilized rare mineral occurrences in the region (Demirmen, 1965). Similar mineral formations have been reported in a case study from the

Troodos Ophiolite Complex, Cyprus (Christidis, 2006). In other related study on trace metal distribution from a serpentinite weathering, Caillaud and his colleagues stated that the distribution of four trace metals (Ni, Cr, Mn and Co), derived from a natural trace metals-bearing rock (serpentinite), are relatively enriched in weathered horizons compared to the rock, in the same way as iron and aluminium whereas magnesium is largely leaching. Silicates (serpentine and clinocllore) contain Cr, Ni and Mn whereas oxides concentrate Co and Cr. In the first weathering stages, Ni and Cr are concentrated in secondary clays, especially in Fe-montmorillonite (derived from serpentine minerals) and in trioctahedral vermiculite (derived from chlorite) respectively, whereas Mn and Co are mainly used to constitute secondary oxides (Caillaud et al., 2009). Franklin and his colleagues stated the remobilized occurrences of chromian clinocllore in the Coolac Serpentinite Belt which is a sub vertical, alpine-type ultramafic body within the Palaeozoic Lachlan Fold Belt of eastern Australia, and additionally, they revealed that chromium was mobilized over a substantial temperature interval for the chrome-bearing phases including ferrochrome, uvarovite (formation temperature 500°C+) and chromian clinocllore (formation temperature ~300°C) (Franklin et al., 1992).

The ICP-AES analysis (Table 3.1) verify that relatively higher concentrations of some transition metal elements, such as Fe (52300 ppm), Cr (44200 ppm), Mn (829 ppm), Ni (812 ppm), V (356 ppm), Zn (303 ppm), Bi (245 ppm), La (90 ppm), Co (68 ppm), Ga (50 ppm), Cu (28 ppm), Sr (23 ppm), and Mo (12 ppm) are unique characteristics of Turkish kammererite. Some of them are certainly responsible for the production of the original magenta color and all kind of luminescence excitation peaks. Manganese provides a lavender color (Nassau and Shigley, 1987). The UV-Vis-NIR absorption spectra (Chadwick, 2008) showed transmission windows in the blue and red portions of the spectrum, which are consistent with the magenta color of the kammererite sample. In addition, Chadwick (2008) stated that the strong absorption peaks near 400 and 550 nm correlated to the features seen in the desk-model spectroscopy, and they were attributed to Cr³⁺ (Burns, 1993). Wight (1996) and Chadwick (2008) stated that two smaller peaks were present at ~680 nm, 685 nm and ~690 nm.

Table 3.1 Chemical bulk and trace element analyses of the Turkish kammererite crystals, as formulized $[(Mg,Fe^{2+})_5(Al,Cr,Fe^{3+})_2Si_3O_{10}(OH)_8]$ according to Zanazzi et al. (2006). Relatively higher concentrations of some main building elements and of some transition metal elements are unique characteristics of kammererite (chromian clinocllore). These characteristic can be provenance, and ascribed to ultrabasic genesis for Turkish kammererite. Some of them are certainly responsible for the production of both the original magenta color and all kind of luminescence excitation peaks.

Oxides %	Instrument (XRF)	Sample	Elements	Instrument (ICP-AES)	Sample
	Detection limits	Kammererite on Chromitite matrix in peridotitic host rock		Detection limits	Kammererite on Chromitite matrix in peridotitic host rock
SiO ₂	0.01 %	6.55			
Al ₂ O ₃	0.01 %	12.43	Al	0.01 % 100 ppm	5.23 52300
Fe ₂ O ₃	0.01 %	15.21	Fe	0.01 % 10 0ppm	8.36 83600
CaO	0.01 %	0.05	Ca	0.01 % 100 ppm	0.03 300
MgO	0.01 %	18.07	Mg	0.01 % 100 ppm	8.71 87100
Na ₂ O	0.01 %	0.05	Na	0.01 % 100 ppm	0.01 100
K ₂ O	0.01 %	0.03	K	0.01 % 100 ppm	<0.01 <100
Cr ₂ O ₃	0.01 %	9.24	Cr	1 ppm	44200
TiO ₂	0.01 %	0.18	Ti	0.01 % 100 ppm	0.07 700
MnO	0.01 %	0.11	Mn	5 ppm	829
P ₂ O ₅	0.001 %	0.008	P	100 ppm	10
SrO	0.01 %	0.01	Sr	1 ppm	23
BaO	0.01 %	0.01	Ba	10 ppm	10
LOI	0.01 %	1.25			
Total	0.01 %	98.20			
			Ag	0.5 ppm	2.0
			As	5 ppm	<5
			Be	0.5 ppm	<0.5
			Bi	2 ppm	245
			Cd	0.5 ppm	<0.5
			Co	1 ppm	68
			Cu	1 ppm	28
			Ga	10 ppm	50
			La	10 ppm	90
			Mo	1 ppm	12
			Ni	1 ppm	812
			Pb	2 ppm	19
			S	0.01 %	0.02
			Sb	5 ppm	<5
			Sc	1 ppm	4
			Th	20 ppm	<20
			Tl	10 ppm	<10
			U	10 ppm	<10
			V	1 ppm	356
			W	10 ppm	10
			Zn	2 ppm	303

3.5 Dispersive (Green Laser) Confocal Micro-Raman (DC μ RS) Spectroscopy

Micro-Raman spectroscopy provides a unique method for characterizing the crystal chemical properties of homogenous samples as well as heterogeneous ones. The technique is now routinely used to establish the identity of an unknown gem, study inclusions, and characterization (Delé-Dubois et al., 1986; Wang et al., 1994; Hanni et al., 1997; Fan et al., 2009). In addition, the spatial resolution and ease of data collection of this technique are particularly useful for rapid identification of minerals in thin section (Mao et al., 1987). Because of the sensitivity of vibrational frequencies and scattering intensities to slight differences in crystal structures (i.e., bond angles, site symmetries, and lattice vibrations), such vibrational spectroscopic methods are also well suited for distinguishing among mineral polymorphs (Lewis and Edwards; 2001; Gopal, 2004; Chao et al., 2010).

The dispersive (green laser) confocal micro-Raman spectra, with C^{\perp} axis {100} (Figure 3.4), as the mapped multi spectra and related microscope image (Figure 3.5), as the single spectrum with C^{\parallel} axis {001} (Figure 3.6), as the mapped multi spectra with C^{\parallel} axis and related microscope image (Figure 3.7), and also as the separated and overlapped of these spectra for the comparison and contrasting with ideal clinocllore Raman data which it was embedded within the spectrometer library (Figure 3.8), of the representative Turkish kammererite sample in the range between 50 and 1600 cm^{-1} were examined to investigate the vibrational and structural characteristics of the component phases, including their spatial distribution. It is important to note that these Raman bands belonging to Turkish kammererite have not been reported in any previous references.

Accordingly, characteristic Raman bands associated with $(\text{MgO}_4)^{6-}$, $(\text{AlO}_4)^{5-}$, $(\text{CrO}_4)^{5-}$, $(\text{FeO}_4)^{5-}$, and $(\text{SiO}_4)^{4-}$ molecules in Turkish kammererite are identified. Dispersive confocal (green laser) micro-Raman spectroscopy (DC μ RS) shows that the strong micro-Raman bands in the samples are peaked at 681, 541, 353, 197, and 112 cm^{-1} . These bands are a result vibrational symmetric and asymmetric stretching and bending modes of many tetrahedral oxy-anions mentioned above, which forms

all kammererite structure which may be formulized as $[\text{Mg}_5(\text{Al,Cr,Fe})_2\text{Si}_3\text{O}_{10}(\text{OH})_8]$ with reference to the abundance of the main oxides in the XRF bulk analysis (Table 3.1).

A total of 13 vibrational micro-Raman bands of Turkish kammererite were established (Figures 3.4 and 3.6). However, five of the bands peaked at about 681, 541, 353, 197 and 112 cm^{-1} are distinctive because of the remarkable differentiations of the relative intensities and positions. They were firstly classified as the main vibrational bands and then possible causes of those in Turkish kammererite were inferred (Table 3.2).

On the other hand, the spectra in Figures 3.4 and 3.6 show a combination of the mapped Raman spectra and related microscope images (Figures 3.5 and 3.7), and also the overlapped and separated Raman spectra which were compared with that of the ideal clinocllore in the library of the device (Figure 3.8).

The most recent technological developments in Raman spectroscopy have enabled rapid mapping. Hyper-spectral imaging, where a Raman mapping of a surface (collection of thousands of spectra) is used to image a physical or chemical property using a data set of parameters extracted by modelling the Raman spectra recorded point-by point (Delé-Dubois et al., 1986; Gouadec and Colombar, 2007; Šontevska et al., 2007 and 2008; Colombar and Prinsloo, 2009; Fan et al., 2009; Carter et al., 2010). Rapid mapping capabilities allow the large-scale survey maps to be collected first and smaller, higher spatial resolution maps obtained once a region of interest has been located. The large-scale map and the related microscope images of Turkish kammererite suggest the existence of the same bands (Figures 3.5 and 3.7). Finally, these bands were matched with the library spectrum of the previously given clinocllore in the spectrometer. The comparison and contrasting with that of the previously given clinocllore crystal of the overlapped micro-Raman bands in the C^\perp and $C\parallel$ spectra shows that the spectra of Turkish kammererite is closely similar to the previously given clinocllore. However, some additional bands are present, since the investigated crystal is a chromium-rich clinocllore (Figure 3.8).

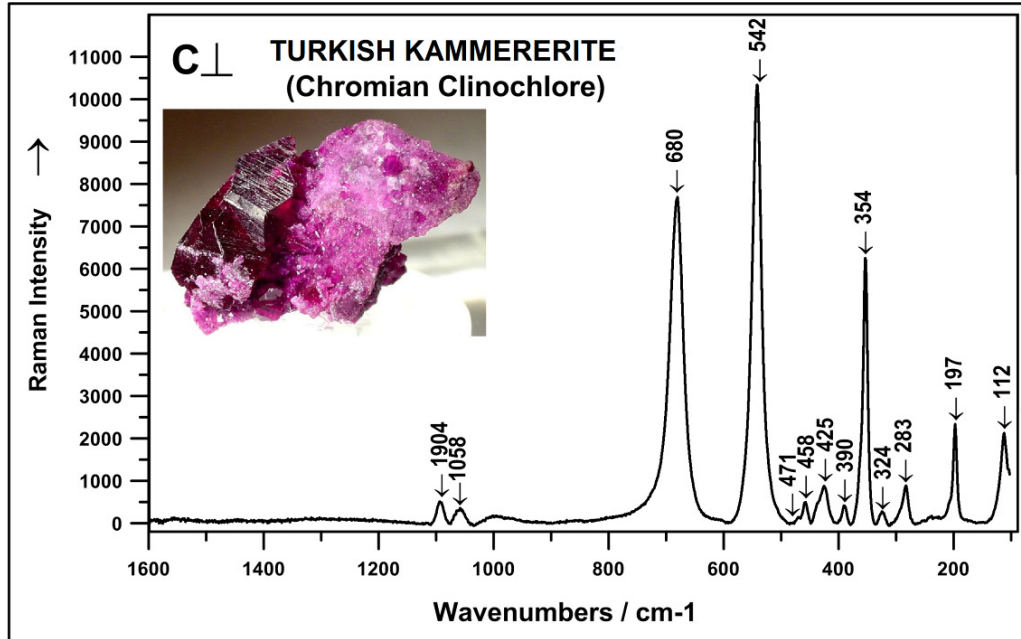


Figure 3.4 The dispersive confocal micro-Raman vibrational bands along the perpendicular to C^\perp [100] axis single spectrum of the representative Turkish kammererite crystal sample. Spectral details are as the followings; Binning: 1, objective: x10, filter: 100%, exposition: 20, accumulation: 5, laser: 532.06, spectro: 949.942, hole: 500, silt: 100, grating: 1800T, ICS correction: on, and power: 15 mW at sample.

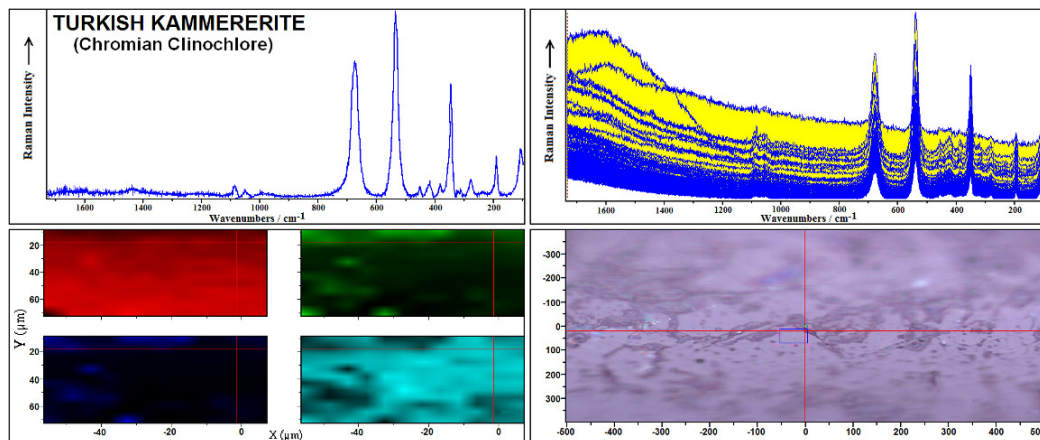


Figure 3.5 The mapped multi spectra along C^\perp axis [100], and the related image being the vertical view with a x50 magnification under the spectrometer microscope, since the kammererite mineral was crystallized on the chromitite matrix in vertical position.

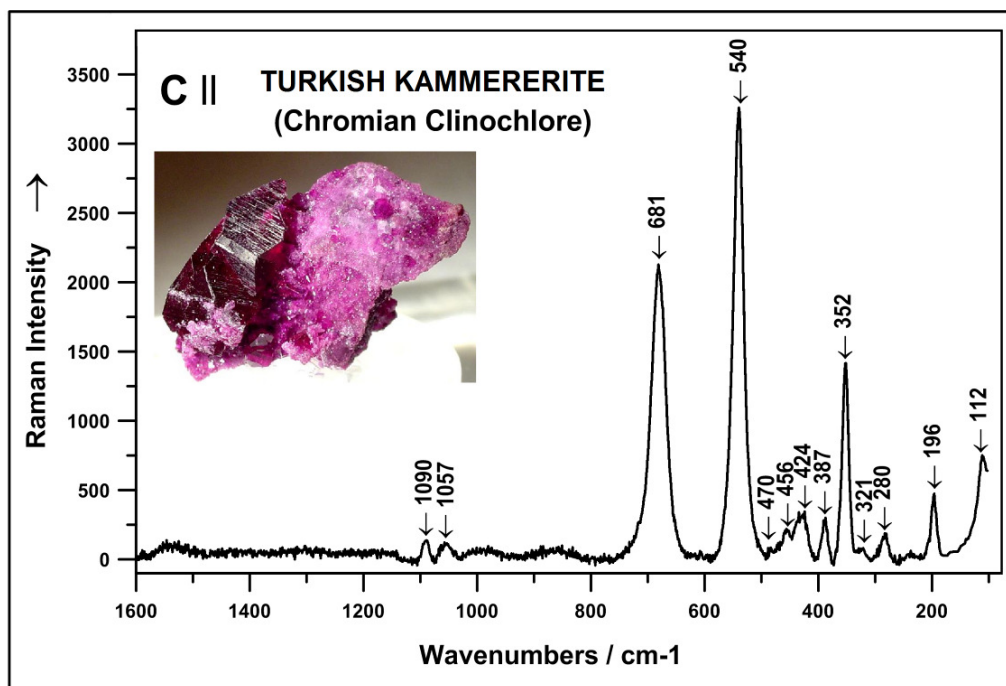


Figure 3.6 The dispersive confocal micro-Raman vibrational bands in the parallel to $C \parallel \{001\}$ axis single spectrum of the representative Turkish kammererite crystal sample. Spectral details are as the followings; Binning: 1, objective: x10, filter: 100%, exposition: 20, accumulation: 5, laser: 532.06, spectro: 949.942, hole: 500, silt: 100, grating: 1800T, ICS correction: on, and power: 15 mW at sample.

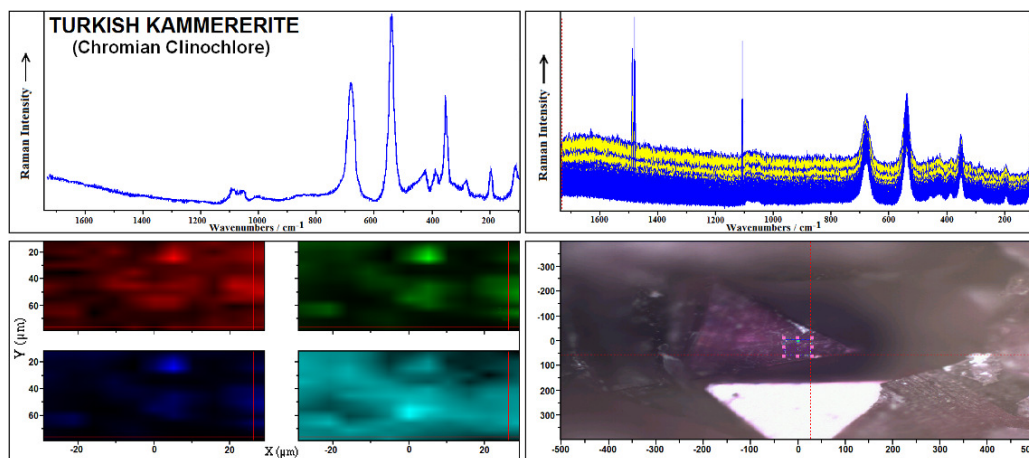


Figure 3.7 The mapped multi spectra with $C \parallel$ axis $\{001\}$, and the related image being the vertical view with a x10 magnification under the spectrometer microscope, since the kammererite mineral was crystallized on the chromite matrix in vertical position.

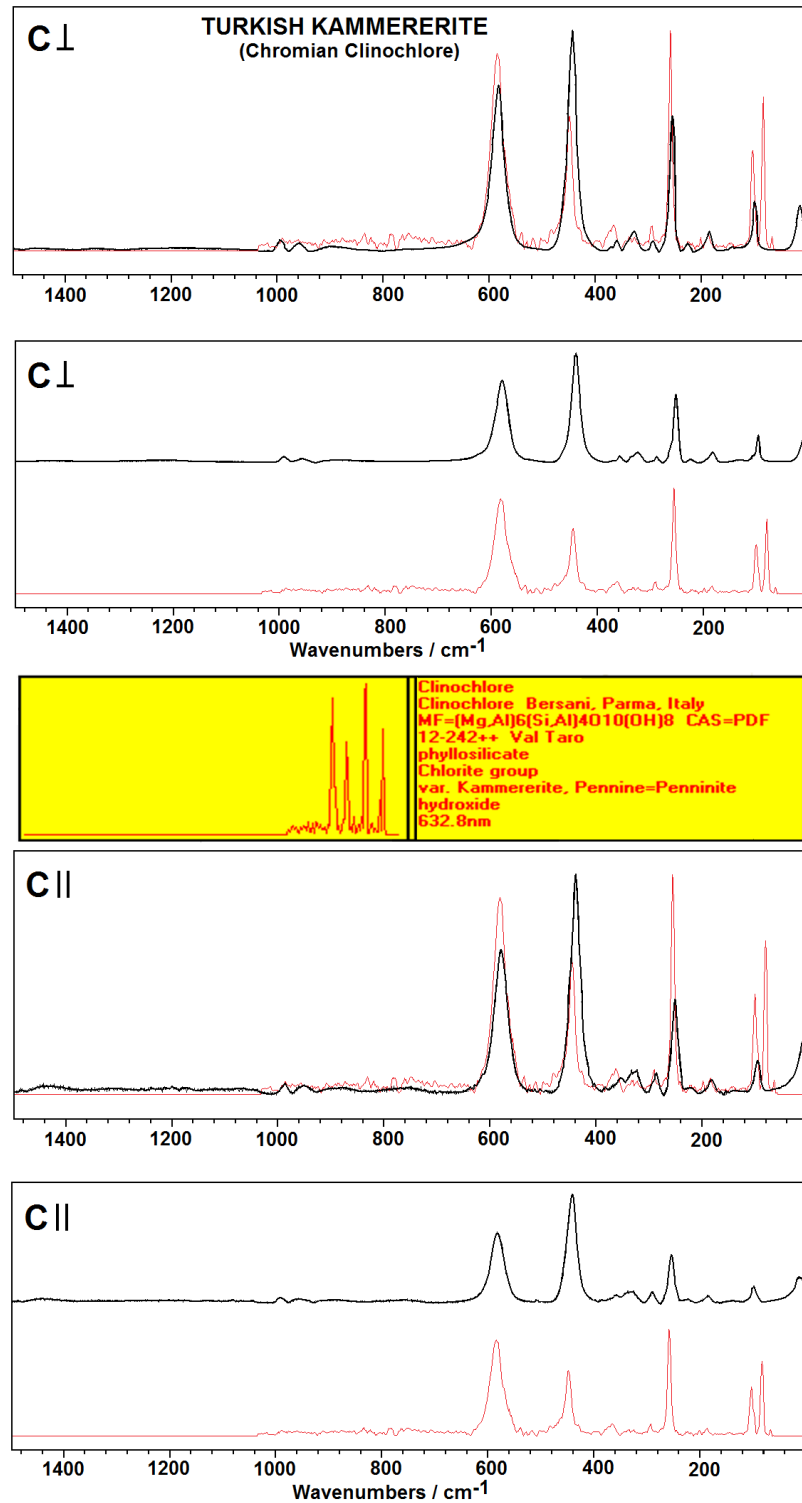


Figure 3.8 The comparison and contrasting with that of the ideal clinchlore crystal of the overlapped micro-Raman bands in the Turkish kammererite spectra with two different axes with those of the ideal clinchlore crystal. The latter were extracted from the spectrometer library.

The presence of abundance of some main building atomic structures in Turkish kammererite, such as $(\text{MgO}_4)^{6-}$, $(\text{AlO}_4)^{5-}$, $(\text{CrO}_4)^{5-}$, $(\text{FeO}_4)^{5-}$, and $(\text{SiO}_4)^{4-}$ can be attributed to extrinsic defects (chemical impurities) (Franklin et al., 1992; Gravel et al., 1997; Šontevska et al., 2007 and 2008), and to intrinsic defects (the nonbridging oxygen deficient centres with several precursors, self-trapped exciton, and dislocations) (Brown, 1976; Berman, 1988; Catti et al., 1995; Gopal, 2004) (Table 3.2).

Table 3.2 Confocal (green laser) micro-Raman vibrational bands of the representative Turkish kammererite with c-perpendicular and c-parallel, and their inferred causes according to symmetry and Raman activity of $(\text{MgO}_4)^{6-}$, $(\text{AlO}_4)^{5-}$, $(\text{CrO}_4)^{5-}$, $(\text{FeO}_4)^{5-}$, and $(\text{SiO}_4)^{4-}$ tetrahedrons with Td symmetry (the inferences were modified from Tossell, 1975; Brown, 1976; Kingma and Hemley, 1994; Colomban and Prinsloo, 2009).

Band Number	Confocal (green laser) Micro-Raman Wavenumbers / cm^{-1}		Inferred Causes
	$C^\perp \{100\}$	$C \parallel \{001\}$	
1	1094	1090	ν_3 doubly asymmetric stretching modes of nonbridging oxygen hole centres with several precursors (i.e., hydroxyl group, peroxy linkage) and oxygen vacancy.
2	1058	1057	
3	680	681	ν_1 single symmetric stretching mode of $(\text{MgO}_4)^{6-}$
4	542	540	ν_2 single symmetric stretching mode of $(\text{CrO}_4)^{5-}$
5	471	470	ν_4 single asymmetric bending modes of degeneracy of $(\text{SiO}_4)^{4-}$
6	458	456	ν_4 single asymmetric bending modes of degeneracy of $(\text{SiO}_4)^{4-}$
7	425	424	ν_4 single symmetric bending modes of degeneracy of $(\text{FeO}_4)^{5-}$
8	390	387	ν_4 single asymmetric bending modes of degeneracy of $(\text{SiO}_4)^{4-}$
9	354	352	ν_4 single symmetric bending modes of degeneracy of $(\text{FeO}_4)^{5-}$
10	324	321	ν_4 single asymmetric bending mode of degeneracy of $(\text{AlO}_4)^{5-}$
11	283	280	ν_4 single asymmetric bending mode of degeneracy of $(\text{AlO}_4)^{5-}$
12	197	196	ν_4 single asymmetric bending modes of degeneracy of $(\text{SiO}_4)^{4-}$
13	112	112	ν_4 single asymmetric bending mode of degeneracy of $(\text{AlO}_4)^{5-}$

The valence region in a crystal structure is separated into a set of predominantly O 2s type orbitals ($4a_1$ and $3t_2$). A set of σ bonding orbitals ($5a_1$ and $4t_2$), and a set of

predominantly O 2p non-bonding orbitals ($5t_2$, $1e$, $1t_1$). The lowest lying empty orbitals are the $6t_2$ and $6a_1$, of mixed Si and O character. The highest energy orbitals are the strongly antibonding $2e$, $1t_2$, and $7a_1$ (Tossell, 1975). The highest energy filled orbital, the $1t_1$, has not been included in the tabulation, because it is uniformly 100% oxygen in character. In $(\text{SiO}_4)^{4-}$, each of the four highest energy orbitals has substantial Si character, although Si participation is clearly greatest for the s-type $5a_1$ orbital. In addition, all the orbitals are predominantly of O 2p character. For the $4t_2$ and $5a_1$ bonding orbitals a substantial fraction of the density lies in the inter-atomic region, indicating strong involvement in chemical bonding (Tossell, 1975). Tossell has expressed that the Metal-Oxygen (M-O) contributing most strongly to the stability of the system is the $5t_2$ σ bonding M-O of Si 3p and O 2p character. Involvement of the Si 3d orbitals in the chemical bond is found to be small. The valance band-conduction band separation also decreases from 10.2 to 6.5 eV along the series and the lowest conduction band orbital changes from central atom p-like to central atom s-like in character. One of the valence molecular orbitals (the $5a_1$, Si 3s-O 2p bonding orbital) rises in energy as the central atom changes from Si to Mg. Thus, it is postulated that the observed instability of $(\text{MgO}_4)^{6-}$ is associated with the high energy of this orbital (Tossell, 1975).

However, the contribution of ionic bonds like Al-O and Mg-O is null according to that of covalent Si-O bonds (Catti et al., 1995; Hofmeister et al., 1999; Colomban and Prinsloo, 2009). Therefore, the considerable strength of the Si-O bond results in a high melting temperature (Colomban and Prinsloo, 2009, Farges, 2009). The basic unit of a silicate, the SiO_4 tetrahedron, is a strong chemical entity and the possibility to share oxygen atoms between two tetrahedrals with variable Si-O-Si angles or to have non-bridging oxygen atoms gives a polymeric character to silicates (Rule and Bailey, 1987; Kleppe et al., 2003; Chao et al., 2010; Ślodziak and Colomban, 2010).

Kammererite (chromian clinochlore), in essence, is one of the rarest clinochlore minerals which is a sub-variety of large family of the chlorite minerals (Lapham, 1958). Even though it is the monoclinic *I1b-2* polytype, with symmetry *C2/m*, which is one of the most abundant regular-stacking one-layer chlorites occurring in nature

(Dietrich and Medenbach, 1978; Bailey, 1988; Joswig and Fuess, 1989; Zheng and Bailey, 1989; Welch and Marshall, 2001; Zanazzi et al., 2007; Chadwick, 2008). Accordingly, the first most intensive Raman band at 542 (540) cm^{-1} is inferred to the ν_2 single symmetric stretching mode of $(\text{CrO}_4)^{5-}$. The second most intensive Raman band at 680 (681) cm^{-1} is inferred to the ν_1 single symmetric stretching mode of $(\text{MgO}_4)^{6-}$. The third most intensive Raman band at 354 (352) cm^{-1} is inferred to the ν_4 single symmetric bending modes of degeneracy of $(\text{FeO}_4)^{5-}$. In addition, there are present two relatively intensive Raman bands as peaked 197 (196) and 112 (112) cm^{-1} . They are inferred to the ν_4 single asymmetric bending modes of degeneracy of $(\text{SiO}_4)^{4-}$, and ν_4 single asymmetric bending mode of degeneracy of $(\text{AlO}_4)^{5-}$, respectively.

As can be inferred from in Table 3.2, the two weak Raman bands of the Turkish kammererite crystals at 1094 (1090) and 1058 (1057) cm^{-1} can be attributed to intrinsic defects (the nonbridging oxygen deficient centres with several precursors and self-trapped exciton) (Parise et al., 1994; Pawley et al., 1995; Pawley et al., 2002). Nutall and Weil (1980) reported a hydrogenic trapped hole-centre with four hydrogen atoms in a regular silicon lattice position. Since, in the case of some elements, compensation of the electric charge is necessary, additional cations such as H, Li, Na., K, Ag, can be incorporated in inter-lattice positions in conjunction with structural channels (Nutall and Weil, 1980). The nonbridging oxygen hole centre ($\equiv\text{Si-O}$) is described as a hole trapped in a single oxygen atom bound to a single silicon on three oxygen atoms in the SiO_2 structure (Nutall and Weil, 1980; Weil, 1984). Oxygen excess centres include the peroxy radical ($\equiv\text{Si-O-O}$), an oxygen associated hole centres consisting of an O^{2-} ion bonded to single silicon on three oxygen atoms, and the peroxy linkage ($\equiv\text{Si-O-O}\equiv$). A further type of defect is OH⁻ centres which consist of a proton bound on a regular lattice O^{2-} ion, located between two O^{2-} ions of the SiO_4 tetrahedron (Słodczyk and Colomban, 2010; Gouadec and Colomban, 2007; Chao et al., 2010; Sontevska et al., 2007 and 2008; Nutall and Weil, 1980; Weil, 1984). Because of the negative net charge, additional trivalent substitutes of the Si^{4+} positions occur as charge compensation (i.e. Al^{3+}) in such a way that an additional proton is bound on the Al^{3+} (Rule and Bailey, 1987; Lapham,

1958; Dietrich and Medenbach, 1978; Colombari and Prinsloo, 2009; Slodczyk and Colombari, 2010; Gouadec and Colombari, 2007).

3.6 Luminescence (PL, CL)

It is well-known that some luminescences were the emission of light from a material when excited by

- UV (photoluminescence, PL)
- Electrons (cathodoluminescence, CL)

Indeed, perfect-structured crystalline materials emit very little light when excited by irradiation and/or heating. Therefore, all kinds of luminescence of minerals (and materials) tell us about the crystalline defects that occur in all natural solids. These are (1) chemical impurities, such as trace elements, (2) structural imperfections, such as vacancies (holes where atoms should be), elements with the wrong charge (O^{1-} where O^{2-} should be), dislocations (where bonds do not join up properly), and (3) many others (Blasse and Grabmaier, 1994; Dean, 1999; Gaft, 2005; Handerson and Imbusch, 2006). Different luminescence centres produced by cathodoluminescence (CL), and photoluminescence (PL) are due to the overall signals of the excitation using irradiation.

During this investigation, three different luminescence spectra of the Turkish kammererite samples [photoluminescence-PL (Figure 3.9) and cathodoluminescence-CL (Figure 3.10) were taken into consideration, and evaluated.

3.6.1 Photoluminescence (PL)

Photoluminescence (PL) excitation emission scans of Turkish kammererite were obtained for the first time in three dimensions (3D) to characterize a variety of the material parameters, and spectral-colored photoluminescence (3D-PL) morphologies and (2D-PL) graphics are given in Figure 3.9. These spectral

characteristics ranging between wavelengths of 300 and 900 nm, and temperatures between 220 and 340 K, are unique to Turkish kammererite.

Accordingly, a total of 3 maxima peaks at 545 nm and at the temperatures of 230, 240, and 250 K respectively, and a total of 3 maxima peaks at 610 nm and at the same temperatures were observed (Figure 3.9).

As seen, three major bands sequence are very distinctive on the spectrum. These bands appear at low temperatures and in the regions of green-yellow and orange only.

In fact, what cause photoluminescence (PL) as well as other luminescence are lattice defects as either chemical impurities or structural imperfections (Blasse and Grabmaier, 1994; Gfroerer, 2000; Gaft et al., 2005; Handerson and Imbusch, 2006). Therefore, individual PL bands appearing at the end of the excitation emission scans at the negative temperature values (mainly 250 K) can be attributed to defects related to some trace element contents. Thus, it can be claimed that the majority of these defects come from cationic substations, since PL spectroscopy provides electrical (as opposed to mechanical) characterization, and it is a selective and extremely sensitive probe of discrete electronic states (Gfroerer, 2000).

On the other hand, in the case of obtaining information on the quality of surfaces and interfaces in Turkish kammererite, it was revealed that the intensity and magnitude of the PL signals readable increase with Fe, Cr, Mn, Ni, V, and Zn implications, which have relatively large cationic radii. Accordingly, this situation at low temperatures can show an electrical charge changing reaction in the silica tetrahedral structure with developing strained Al(Si)-O-Fe, Al(Si)-O-Cr, Al(Si)-O-Mn, Al(Si)-O-Ni, Al(Si)-O-V, and Al(Si)-O-Zn bonds.

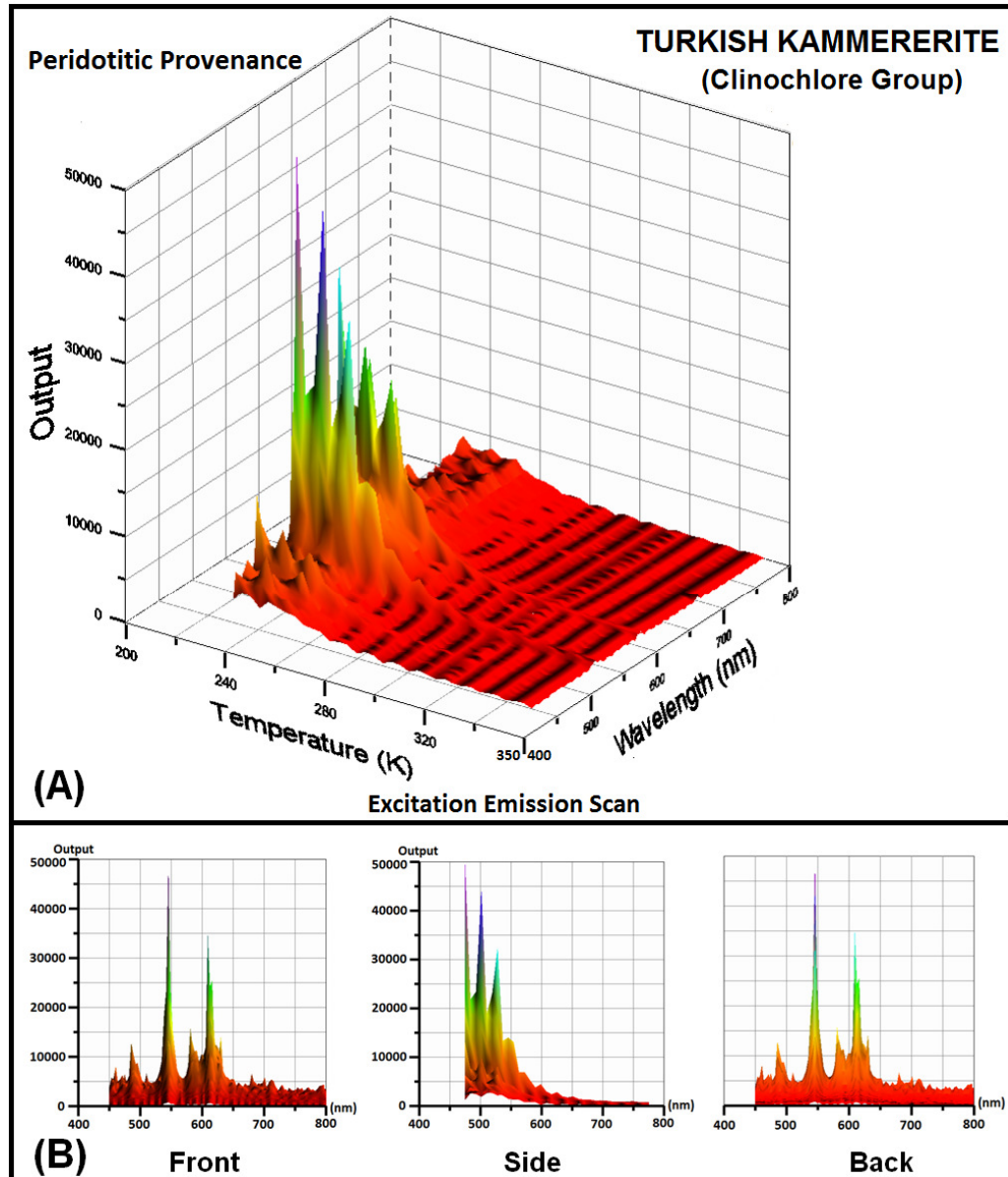


Figure 3.9 Spectral-colored photoluminescence (3D-PL) morphologies and (2D-PL) graphics of the representative Turkish kammererite sample; from the right-viewed front perspective (3D-PL) (A), the left-viewed back perspective (3D-PL) (B), the emission versus the wavelength graphic (2D-PL) (C), the emission versus temperature graphic (2D-PL)(D). Major maxima peaks in the visible and near-infrared regions are measured about at 398, 413, 427, and 740 nm respectively.

3.6.2 Cathodoluminescence (CL)

Cathodoluminescence (CL-2D) spectra at room temperature produced by AC at 24 keV energy display individual luminescence patterns in the representative Turkish kammererite sample (Figure 3.10).

The cathodoluminescence AC experimental data at 24 keV energy show that one major wide spectral emission band appears at readable intensity and magnitude at 90 Hz in the red wavelength region at 730 nm (Figure 3.10). In addition, because the intensities of the spectral CL emission bands at the other frequencies are very low, they can be discarded.

Accordingly, a relationship can be observed between the CL emissions and presence of some transition metal elements. Formation of the CL bands can be observed when different excitation modulation frequencies are used. However, it is obvious that not all trace elements play a direct role.

It can be seen that the peaks at all frequencies decrease sharply as the excitation modulation frequency increases. The fact that such changes are apparent at the very low frequencies of modulation immediately indicates that there are some very long lifetime processes occurring. This situation at room temperature can show a mechanical changing reaction in the silica structure. When the CL luminescence activators of Turkish kammererite are considered, it is obvious that the peak-wavelengths and intensities of CL are highly dependent on the spatially varying concentrations of metal trace impurities.

As a result, it can be suggested that the remarkable CL luminescence emission in the red wavelength region (at 730 nm) in Turkish kammererite is probably due to the metal-oxygen in the $(\text{MgO}_4)^{6-}$, $(\text{AlO}_4)^{5-}$, $(\text{CrO}_4)^{5-}$, $(\text{FeO}_4)^{5-}$, and $(\text{SiO}_4)^{4-}$ tetrahedrons. These strained structures with O–OH bonds stabilise some non-bridging oxygen vacancy hole centres which seem to be ultimately responsible for this kind of electron excitation.

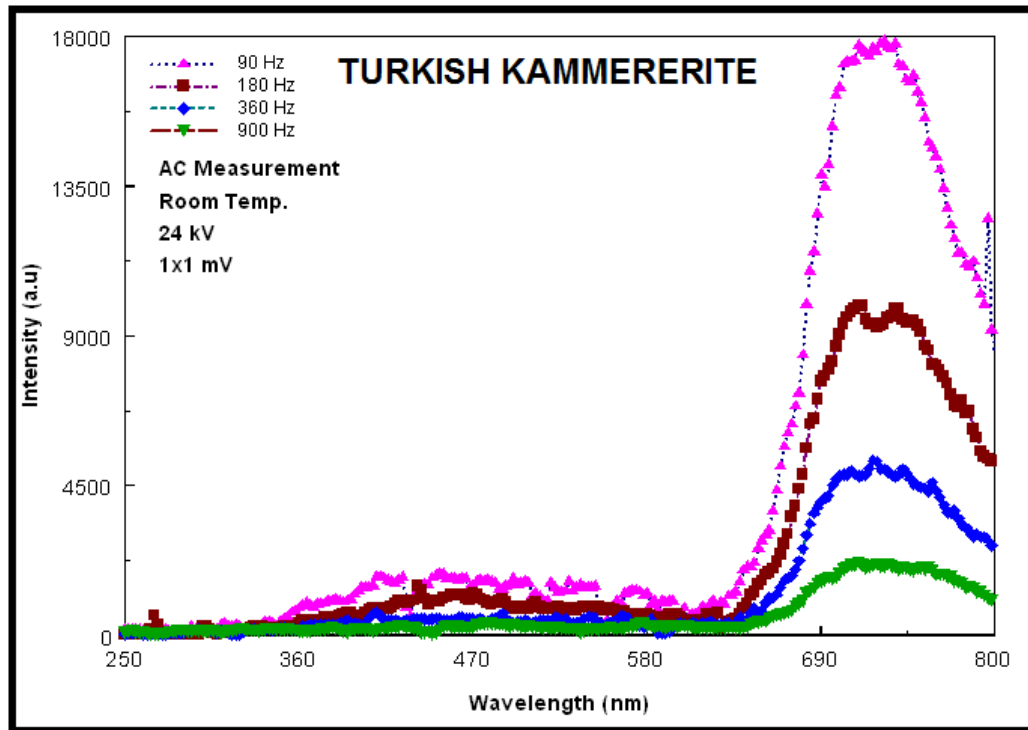


Figure 3.10 AC cathodoluminescence (CL) spectra at 24 keV energy and 300 K temperature of the representative Turkish kammererite sample. One major spectral emission band appears in readable intensity and magnitude at 90 Hz in the visible wavelength region (red region) at about 730 nm.

CHAPTER FOUR

CONCLUSIONS

Meanwhile, since kammererite (chromian clinochlore) has a low hardness (Mohs 2–2.5) and a perfect cleavage, it is not very suitable for use in common jewellery, but is typically sold as crystal specimens and/or as a collector's stone. However, some faceted gems have been exhibited as both loose stones and mounted on special jewellery. Therefore, when a kammererite crystal can be faceted and cabochon cut, it is highly valued on the gem market. Thus, it is necessary to collect some reliable non-destructive and non-invasive characterization data of these highly prized natural specimens, in order to distinguish them from synthetic and color-enhanced ones.

This study focuses on kammererite identification and on the evaluation of the composition, provenance, and genesis of this kind of chromian clinochlore.

An application of dispersive (visible) confocal micro-Raman spectroscopy (DC μ RS) with a silicon CCD array was carried out as a non-destructive and non-invasive method to reveal the natural mineralogical characterization and provenance of Anatolian kammererite and to distinguish it from other synthetic, simulated and color enhanced clinochlores. The dispersive confocal micro-Raman vibrational shifts of a gem-quality Turkish kammererite single crystal were observed for the first time in combination with X-ray fluorescence (XRF) and inductive coupled plasma-atomic emission spectroscopy (ICP-AES) for analyses and detections. A total of 13 vibration shifts of kammererite were established, and their causes were inferred. In addition, the rapid mapping capabilities allow for large-scale survey maps to be collected with smaller higher spatial resolution maps obtained once a region(s) of interest has been located. This technology has been used to investigate the Turkish kammererite crystals.

Photoluminescence to be depended on the changing excitation and temperature emitted the some defects that exist in Turkish kammererite. The PL spectroscopy indicates that the 3D morphological changes similar which were caused by ultraviolet excitation during the increasing temperature give us insights into readily

differentiations of provenance and genesis of the investigated minerals. Hence, a total of 3 maxima peaks at 545 nm and at the temperatures of 230, 240, and 250 K respectively, and a total of 3 maxima peaks at 610 nm and at the same temperatures were observed in Turkish kammererite. These bands appear at low temperatures and in the regions of green-yellow and orange only.

The CL study summarizes results of extensive cathodoluminescence study on Turkish kammererite. CL can be used in a purely descriptive way to detect kammererite of different origin or to reveal processes of crystal growth, recrystallization, alteration or diagenesis by variable CL colours. On the other hand, CL is an effective method for spatially resolved analysis of point defects in kammererite by spectral measurements. In combination with trace-element analysis, the different emission bands can be related to specific lattice defects in the kammererite structure. The defects causing different CL emissions often reflect the specific physico-chemical conditions of crystal growth and therefore, can be used as a signature of genetic conditions. The remarkable CL luminescence emission in the red wavelength region (at 730 nm) in Turkish kammererite is probably due to the metal-oxygen in the $(\text{MgO}_4)^{6-}$, $(\text{AlO}_4)^{5-}$, $(\text{CrO}_4)^{5-}$, $(\text{FeO}_4)^{5-}$, and $(\text{SiO}_4)^{4-}$ tetrahedrons.

On the other hand, the magenta coloration of the Turkish kammererite crystals is also very individual. Chadwick (2008) reported that optic absorptions obtained with UV-Vis-NIR spectroscopy showed some transmission windows in the blue and red portions of the spectrum, which are consistent with the magenta color of the samples. The unique magenta coloration of the Turkish kammererite crystals is due to a complex mechanism, since many transition metals, which are coloration agents, are present. Some of the elements Fe, Cr, Mn, Bi, Co, Cu, Mo, Ni, V, and Zn are certainly responsible as external lattice defects for producing the unique purple color, but in order to clarify the magenta color formation in these crystals, further investigation will be necessary.

REFERENCES

- AMCSD (2012). *American Mineralogist crystal structure database by Downs et al.* (1993) via. <http://www.minsocam.org/MSA/Crystal_Database.html and <http://ruff.geo.arizona.edu/AMS/amcsd.php>>.
- Arem, J.E. (1987). *Color Encyclopaedia of Gemstones, 2nd Ed.* Van Nostrand Reinhold. Co., New York.
- Back, M. & Mandarino, J. (2008). *Fleischer's Glossary of Mineral Species, 10th Ed.* The Mineralogical Record, Inc., Tucson.
- Bailey, S.W. (1988) Chlorites: structures and crystal chemistry. In S.W. Bailey Ed., *Hydrous Phyllosilicates (exclusive of micas)*, 19, p. 347-403. *Reviews in Mineralogy and Geochemistry*, Mineralogical Society of America, Chantilly, Virginia.
- Berman, R.G. (1988) Internally consistent thermodynamic data for minerals in the system Na₂O-K₂O-CaO-MgO-FeO-Fe₂O₃-Al₂O₃-SiO₂-TiO₂-H₂O-CO₂. *Journal of Petrology*, 29, 445-552.
- Bersani, D. & Lottici, P.P. (2008). Application of Raman spectroscopy to gemology. *Analytical and Bioanalytical Chemistry*, 397, 2631-2646.
- Blasse, G. & Grabmaier, B.C. (1994). *Luminescent Materials*. Springer-Verlag, 232.
- Brown, B.E., Bailey & S.W. (1963). Chlorite polytypism: II. *Crystal structure of a one-layer Cr-chlorite*. *American Mineralogist*, 48, 42-45.
- Brown, I.D. (1976). On the Geometry of O-H...O Hydrogen Bonds. *Acta Crystallographica*, A32, 24.31.

- Burns, R.G. (1993). *Mineralogical applications of crystal field theory*. Cambridge University Press, London., 551.
- Caillaud, J., Proust, D., Philippe, S., Fontaine, C. & Fialin, M. (2009). Trace metals distribution from a serpentinite weathering at the scales of the weathering profile and its related weathering microsystems and clay minerals. *Geoderma*, 149, 199-208.
- Catti, M., Ferraris, G., Hull, S. & Pavese, A. (1995). Static compression and H disorder in brucite, Mg(OH)₂, to 11 GPa: a powder neutron diffraction study. *Physics and Chemistry of Minerals*, 22, 200-206.
- Carter, E.A., Pasek, M.A., Smith, T., Kee, T.P., Hines, P. & Edwards, H.G.M. (2010). Rapid Raman mapping of a fulgurite. *Analytical and Bioanalytical Chemistry*, 397, 2647–2658.
- Chadwick, K.M. (2008). Chromium-rich clinochlore (kammererite) from Turkey. *Gems and Gemology*, 44, 168-169.
- Chao, X.I.E. Jian-Guo, D.U. Ying, L.I. Yue-Ju, C.U.I. Zhi, C.H.E.N. & Jing, L.I. (2010). Characteristics of Raman Spectra of Natural Clinochlore at 200 °C and 0.95~7.70 GPa. *Spectroscopy and Spectral Analyses*, 30 (12), 3232-3235.
- Colomban, P. & Prinsloo, L. (2009). Optical spectroscopy of silicates and glasses. In: Yatwood, J., Douthwaite, R., Duckett, S. (Eds.), *Spectroscopic Properties of Inorganic and Organometallic Chemistry*, vol. 40. RSC Publishing, 128–149.
- Christidis, G.E. (2006) Genesis and compositional heterogeneity of smectites. Part III. Alteration of basic pyroclastic rocks. A case study from the Troodos Ophiolite Complex, Cyprus. *American Mineralogist*, 91, 685-701.

- Dean, J.A. (1999). *Lange's Handbook of Chemistry, 15th ed.* Mc-Graw-Hill, Inc. New York, 743-772.
- Deckert, V., George, M.W. & Umapathy, S. (2008). Raman spectroscopy at the beginning of the twenty-first century II. *Journal of Raman Spectroscopy*, 39, 1508–1511.
- Delé-Dubois, M.L., Dhamelincourt, P., Poirot, J.P. & Schubnel, H. J. (1986). Differentiation between gems and synthetic minerals by laser Raman microspectroscopy. *Journal of Molecular Structure*, 143, 135-138.
- Demirmen, F. (1965). *Çayırlı ilçesi (Erzincan civarı) genel jeolojisi ve petrol olanakları. M.T.A. (Turkey) Report No: 4845, 16 (in Turkish, unpublished).*
- Dietrich, R. & Medenbach, O. (1978). Kämmererite from the Kop krom mine, Kop Dağları (Turkey). *Mineralogical Record*, 9, 277-287.
- Fan, J.L., Guo, S.G. & Liu, X.L. (2009). The Application of confocal micro-Raman spectrometer to nondestructive identification of filled gemstones. *Spectroscopy Letters*, 42, 129–135.
- Farges, F. (2009). Chromium speciation in oxide-type compounds: application to minerals, gems, aqueous solutions and silicate glasses. *Physics and Chemistry of Minerals*, 36, 463-481.
- Franklin, B.J., Marshall, B., Graham, I.T. & McAndrew, J. (1992). Remobilization of PGE in podiform chromitite in the coolac serpentinite belt, southeastern Australia. *Aust. Journal of Earth Sciences*, 39, 365-371.
- Gaft, M., Reisfeld, R. & Panczer, G. (2005). *Luminescence Spectroscopy of Minerals and Materials, 1^{Ed.}*. Springer, Berlin, 456.

- Gfroerer, T.H. (2000). *Photoluminescence in Analysis of Surfaces and Interfaces in Encyclopedia of Analytical Chemistry*, R.A. Meyers (Ed.), John Wiley & Sons Ltd, Chichester, 9209–9231.
- Gopal, N.O. Narasimhulu, K.V. & Lakshmana Rao, J. (2004). Optical absorption, EPR, infrared and Raman spectral studies of clinocllore mineral. *Journal of Physics and Chemistry of Solids.*, 65(11), 1887-1893.
- Gouadec, G. & Colomban, P. (2007). Raman spectroscopy of nanomaterials: how spectra relate to disorder, particle size and mechanical properties. *Progress in Crystal Growth and Characterization of Materials*, 53, 1–56.
- Götze J. (2000). Cathodoluminescence microscopy and spectroscopy in applied mineralogy. *Freiberger Foschungshefte*, 128-132.
- Grevel, K., Fasshauer, D.W. & Erzner, S. (1997) New compressibility data for clinocllore, kyanite, Mg-chloritoid and Mg-staurolite. *European Journal of Mineralogy*, 1, 138.
- Gucsik, A., (Ed.). (2009). Micro-Raman spectroscopy and luminescence studies in the earth and planetary sciences. In: Gucsik, A. (Ed.), *Proceedings of the International Conference Spectroscopy 2009*, Mainz, Germany, 2–4 April, 2009, 1163 (250).
- Habermann, D. (2002). Quantitative cathodoluminescence (CL) spectroscopy of minerals: possibilities and limitations. *Mineralogy and Petrology*, 76, 247-259.
- Handerson, B. & Imbusch, G.F. (2006). *Optical Spectroscopy*. Oxford University Press, 672.
- Hanni, H., Kiefert, L. & Chalain, J.P. (1997). Raman spectroscopic applications to gemmology. *Journal of Gemmology*, 25, 394-407.

- Hayes, J.B. (1970). Polytypism of chlorite in sedimentary rocks. *Clays and Clay Minerals*, 18, 285-306.
- Hofmeister, A.M., Cynn, H., Burnley, P.C. & Meade, C. (1999). Vibrational spectra of dense, hydrous magnesium silicates at high pressure: Importance of hydrogen bond angle. *American Mineralogist*, 84, 454-464.
- Joswig, W. & Fuess, H. (1989). Neutron diffraction study of a one-layer monoclinic chlorite. *Clays and Clay Minerals*, 37, 511-514.
- Kadayıfçı, H. & Kolaylı, H. (2009). *Geochemical characteristics of podiform chromite ores from the ultramafic massif of Karadağ (northeastern ophiolitic belt, Turkey)*. *Goldsmith Conference Abstracts*, A611.
- Kleppe, A.K., Jephcoat, A.P. & Welch, M.D. (2003). The effect of pressure upon hydrogen bonding in chlorite: a Raman spectroscopic study of clinocllore to 26.5 GPa. *American Mineralogist*, 88, 567-573.
- Komov, I.L., Lukashev, A.N. & Koplus, A.V. (1994). *Geochemical methods of prospecting for non-metallic minerals*. VSP BV: The Netherlands.
- Lapham, D.M. (1958). Structural and chemical variation in chromium chlorite. *American Mineralogist*, 43, 921-956.
- Lewis, I.R. & Edwards, H.G.M. (2001). *Handbook of Raman spectroscopy, from the research laboratory to the process line*. Practical Spectroscopy Series. Marcel Dekker Inc., New York.
- Mao, H.K., Hemley, R.J. & Chao, E.C.T. (1987). The application of micro-Raman spectroscopy to analysis and identification of minerals in thin section. *Scanning Microscopy*, 1, 495-501.

- Marshall, D.J. (1988). *Cathodoluminescence of geological material*. Unwin Hyman, Boston, 345.
- Mitchell, R.S. (1979). *Mineral Names What do They Mean*. N.A.G. Press Ltd., New York.
- M.T.A. (1966). *Chromitite deposits of Turkey. M.T.A. Report No: 132, Ankara (in Turkish)*, 23.
- Nassau, K. & Shigley, J.E. (1987). A study of the general electric synthetic jadeite. *Gems & Gemology*, 23, 27-35.
- Nuttall, R.H.D. & Weil, J.A. (1980). Two hydrogenic trapped-hole species in quartz. *Solid State Commun.*, 33, 99-102.
- Okay, A.D. & Şahintürk, Ö. (1997). *Geology of the Eastern Pontides*. In; Robinson, A.G., (ed) *Regional and Petroleum Geology of the Black Sea and Surrounding Region. AAPG Mem.*, 68, 291-311.
- Özener, H., Arpat, E., Ergintav, S., Doğru, A., Çakmak, R., Turgut, B. & Doğan, U. (2010). Kinematics of the eastern part of the North Anatolian Fault Zone. *Journal of Geodynamics*, 49, Sp. Iss. 141-150.
- Parise, J.B., Leinenweber, K., Weidner, D.J., Tan, K. & Von Dreele, R.B. (1994). Pressure-induced H bonding: Neutron diffraction study of brucite, Mg(OD)₂, to 9.3 GPa. *American Mineralogist*, 79, 193-196.
- Pawley, A.R., Redfern, S.A.T. & Wood, B.J. (1995) Thermal expansivities and compressivities of hydrous phases in the system MgO-SiO₂-H₂O: talc, phase A and 10 Å phase. *Contributions to Mineralogy and Petrology*, 122, 301-307.

- Pawley, A.R., Clark, S.M. & Chinnery, N.J. (2002). Equation of state measurements of chlorite, pyrophyllite, and talc. *American Mineralogist*, 87, 1172-1182.
- Petrascheck, W.E. (1958). Doğu Türkiye krom ihtiva eden ofiyolitlerinin jeolojisi hakkında. *Bulletin of M.T.A. (Turkey)*, 50, 1-15 (in Turkish).
- Raman, C.V. & Krishnan, K.S. (1928). A new type of secondary radiation. *Nature*, 121, 501.
- Rızaoğlu, T., Parlak, O., Hoeck, V. & Dsler, F.(2006). Nature and significance of Late Cretaceous ophiolitic rocks and their relation to the Baskil granitic intrusions of the Elazığ region, SE Turkey. In; Robertson, A.H.F., Mountrakis, D., (eds) *Tectonic Development of the Eastern Mediterranean Region*, Geological Society Special Publication, 260, 327-351.
- Rice, S., Roberson, A.F.H. & Ustaömer, T. (2006). *Late Cretaceous-Early Cenozoic tectonic evolution of the Eurasian active margin in the Central and Eastern Pontides, northern Turkey*. In; Robertson, A.H.F., Mountrakis, D., (eds) *Tectonic Development of the Eastern Mediterranean Region*, Geological Society Special Publication 260, 413-446.
- Rule, A.C. & Bailey, S.W. (1987). Refinement of the crystal structure of a monoclinic ferroan clinocllore. *Clays and Clay Minerals*, 35, 129-138.
- RRUFF. 2012. Database of Raman spectroscopy, X-ray diffraction and chemistry of minerals via, Retrived Mar 22, 2012, from <http://rruff.info/clinchlore/names/asc/>
- Schumann, W. (1984). *Gemstone of the World*. Sterling Publishing Co., N.A.G. Press Ltd., New York.

- Slodczyk, A. & Colomban, P. (2010). Probing the nanodomain origin and phase transition mechanisms in (un) poled PMN-PT single crystals and textured ceramics. *Material*, 3, 5007-5029.
- Šontevska, V. Jovanovski, G. & Makreski, P. (2007). Minerals from Macedonia. Part XIX. Vibrational spectroscopy as identificational tool for some sheet silicate minerals. *Journal of Molecular Structure*, 834-836, 318-327.
- Šontevska, V. Jovanovski, G. Makreski, P. Raskovska, A. & Soptrajanov, B. (2008). Minerals from Macedonia. XXI. vibrational spectroscopy as identificational tool for some phyllosilicate minerals. *Acta Chimica Slovacia*, 55, 757-766.
- Şengör, A.M.C. & Yılmaz, Y. (1981). Tethyan evolution of Turkey: a plate tectonic approach. *Tectonophysics*, 75, 131-241.
- Temiz, H., Guezou, J.C., Tatar, O., Ünlügenç, U.C. & Poisson, A. (2002). Tectonostratigraphy of the Tercan-Çayırılı basin: Implications for the Neogene–Quaternary tectonic deformation of the northeast Anatolian block, Turkey. *International Geology Review*, 44, 243–253.
- Theye, T., Parra, T. & Lathe, C. (2003). Room temperature compressibility of clinocllore and chamosite. *European Journal of Mineralogy*, 15, 465-468.
- Tossell, J.A (1974). Electronic structures of silicon, aluminum, and magnesium in tetrahedral coordination with oxygen from SCF-X.alpha. MO calculations. *Journal of the American Chemical Society*, 97 (17), 4840–4844.
- Townsend P.D. & Rowlands A.P. (2000). *Information encoded in cathodoluminescence emission spectra*, in: M Pagel, V. Barbin, P. Planc, D. Ohnenstetter (Eds), ‘‘Cathodoluminescence in Geosciences’’, Springer Berlin, 41-57.

- Vandenabeele, P. (2010). Raman spectroscopy. *Analytical and Bioanalytical Chemistry*, 397, 2629–2630.
- Walker, J.R. (1989). Polytypism of chlorite in very low-grade metamorphic rocks. *American Mineralogist*, 74, 738-743.
- Wang, A., Han, J., Guo, L., Yu, J. & Zeng, P. (1994). Database of standard Raman spectra of minerals and related inorganic crystals. *Applied Spectroscopy*, 48, 959–968.
- Webmineral. (2012). Minerals arranged by X-ray powder diffraction, Retrived Jan 10, 2012, from <http://webmineral.com/MySQL/xray.php>.
- Weiss, Z., Rieder, M. & Chmielová, M. (1992). Deformation of coordination polyhedra and their sheets in phyllosilicates. *European Journal of Mineralogy*, 4, 665-682.
- Welch, M.D. & Marshall, W.G. (2001). High-pressure behavior of clinocllore. *American Mineralogist*, 86, 1380-1386.
- Welch, M.D. & Crichton, W.A. (2002). Compressibility of clinocllore to 8 GPa at 298 K and a comparison with micas. *European Journal of Mineralogy*, 14, 561-565.
- Welch, M.D., Kleppe, A.K. & Jephcoat, A.P. (2004). Novel high-pressure behavior in chlorite: A synchrotron XRD study of clinocllore to 27 GPa. *American Mineralogist*, 89, 1337-1340.
- Weil, J.A. (1984). A review of electron spin spectroscopy and its application to the study of paramagnetic defects in crystalline quartz. *Physics and Chemistry of Minerals*, 10, 149-165.

- Wight, W. (1996). Check-list for rare gemstones—Kammererite. *Canadian Gemmologist*, 17, 14–17.
- Uysal, D., Tarkian, M., Sadiklar, M.B. & Şen, C. (2007). Platinum-group-element geochemistry and mineralogy of ophiolitic chromitites from the Kop Mountains, northeastern Turkey. *Canadian Mineralogist*, 45, 355-377.
- Zanazzi, P.F. & Pavese, A. (2002). Behavior of micas at high pressure and high temperature. In A. Mottana, F.P. Sassi, J.B. Thompson, Jr., and S. Guggenheim, Eds., *Micas: Crystal Chemistry and Metamorphic Petrology*, 46, p. 99.116. *Reviews in Mineralogy and Geochemistry*, Mineralogical Society of America, Chantilly, Virginia.
- Zanazzi, P.F., Montagnoli, M., Nazzareni, S. & Comodi, P. (2006). Structural effects of pressure on triclinic chlorite: A single-crystal study. *American Mineralogist*, 91, 1871.1878.
- Zanazzi, P.F., Montagnoli, S., Nazzareni, S. & Comodi, P. (2007). Structural effects of pressure on monoclinic chlorite: A single-crystal study. *American Mineralogist*, 92, 655-661.
- Zheng, H. & Bailey, S.W. (1989). Structures of intergrown triclinic and monoclinic IIb chlorites from Kenya. *Clays and Clay Minerals*, 37, 308.316.